ELSEVIER

Tectonophysics 303 (1999) 1–27

TECTONOPHYSICS

Crystallographic preferred orientations and misorientations in some olivine rocks deformed by diffusion or dislocation creep

Timon F. Fliervoet [a,1], Martyn R. Drury [b,*], Prame N. Chopra [c]

[a] *Bayerisches Geoinstitut, Universität Bayreuth, D-95440, Bayreuth, Germany*
[b] *Geodynamics Research Institute, Faculty of Earth Sciences, Utrecht University, PO Box 80.021, 3508TA Utrecht, Netherlands*
[c] *National Key Centre for the Geological Evolution and Metallogeny of Continents, Department of Geology, Australian National University, Canberra, ACT 0200, Australia*

Accepted 30 October 1998

Abstract

The development of crystallographic preferred orientations (CPO) and grain misorientation distributions (MOD) in fine-grained (0.5–30 μm) olivine rocks, experimentally deformed by diffusion creep and dislocation creep has been investigated. The use of electron back-scattered diffraction (EBSD), in a scanning electron microscope (SEM), has enabled the measurement of CPO in rocks which are too fine-grained to be measured by conventional U-stage methods. Our objective is to study the influence of deformation and recrystallisation mechanisms on the CPO and MOD. The olivine rocks studied were deformed in uni-axial compression, in a gas-medium apparatus, to 17–24% strain at temperatures of 1200–1300ºC and 300 MPa confining pressures. The samples show a trend of weaker CPO with lower flow stress which may be related to an increasing component of grain boundary sliding and diffusion creep. In the diffusion creep regime the CPO and MOD are weak to random, whereas in the dislocation creep regime the CPO and MOD are non-random but the MOD is principally controlled by the CPO. These results confirm the idea, based on studies from metals, that the CPO and MOD in olivine are characteristic of the deformation mechanism. Dynamic recrystallisation during dislocation creep results in the occurrence of more intermediate-angle (10–40º) grain boundaries than expected from the CPO. In local areas of complete recrystallisation the MOD is controlled by the CPO which implies that the statistical MOD retains no signature of the initial recrystallisation process. In the dislocation creep regime small grains have a weaker CPO compared to large grains. This result is consistent with predictions from deformation mechanism maps which indicate that the fine recrystallised grains deform by a combination of dislocation creep and grain boundary sliding. The grain boundaries found in the deformed olivine polycrystals are predominately high-angle boundaries with misorientations between 60 and 117º. No obvious evidence has been found for the occurrence of preferred misorientation, or special, grain boundaries.

Keywords: olivine; grain boundaries; texture; misorientations; deformation; dynamic recrystallisation; electron back-scattered diffraction

* Corresponding author: Tel.: +31 030 2531199; Fax: +31 030 2537725; E-mail: martynd@earth.ruu.nl
[1] Present address: Philips Electron Optics, Building AAE, Achtseweg Noord 5, P.O. Box 218, 5600MD Eindhoven, The Netherlands.

0040-1951/99/$ – see front matter
PII: S0040-1951(98)00250-9

1. Introduction

Measurement of textures or crystallographic preferred orientations (CPO) in rocks can provide information on the kinematics and mechanisms of ductile deformation and information on the anisotropy of physical properties in the Earth. For instance, a weak or random CPO is commonly taken as evidence for deformation by grain-size-sensitive (diffusion) creep (e.g. Padmanabhan and Davies, 1980; Karato, 1988; Rutter et al., 1994). Strong CPOs are regarded as arising from dislocation creep (e.g. Nicolas and Poirier, 1976; Knipe, 1989). Dynamic recrystallisation will also affect the microstructure and CPO in a material (Kamb, 1959; Avé Lallemant and Carter, 1970; Duval, 1979; Burg et al., 1986; Karato, 1988; Jessel and Lister, 1990; Wenk et al., 1997).

The bulk CPO can be measured by X-ray or neutron diffraction (Wenk, 1985). Alternatively, the orientation of, large numbers of, individual grains can be measured using various microscopy techniques which enable a direct correlation between the microstructure and the lattice orientation. Such 'discriminatory' CPO analysis (Lloyd and Ferguson, 1986; Lloyd et al., 1987; Randle, 1992, 1993; Lloyd et al., 1997) can also be used to characterise the crystallographic parameters of grain boundaries. These parameters include the orientation of the boundary plane with respect to each grain and the misorientation (rotation axis and angle) of the crystal lattice across the boundary.

Currently there is very little data on grain misorientation distributions (MOD) in rocks and rock texture analysis has mainly concentrated on 'bulk' CPO. Grain boundary misorientation distributions are interesting because they may provide information on the processes involved in the formation of a microstructure. Furthermore, the physical properties of individual grain boundaries are strongly influenced by their crystallography (see Palumbo and Aust, 1992; Randle, 1992, 1993; Wolf and Merkle, 1992). This means that the effect of the grain boundary network on the physical properties of a rock will depend on the grain boundary misorientation relations.

Recent advances in Scanning Electron Microscopy (SEM) have enabled discriminatory CPO measurements to be made in very fine-grained materials using Orientation Contrast Imaging (OCI) and Electron Back-Scatter Diffraction (EBSD) patterns (Gottstein, 1992; Randle, 1992, 1993; Prior et al., 1996). We report the results of a study of the CPO and grain misorientation distributions in some experimentally deformed fine-grained (0.5–30 μm) olivine rocks using the EBSD technique. We compare these results with data obtained from some coarse-grained naturally deformed olivine rocks using light microscopy. The main objective of the study is to investigate the influence of deformation and recrystallisation mechanisms on CPO and grain misorientation distributions in upper mantle rocks.

1.1. Terminology

Many terms have been used in the geological and materials science literature to describe the analysis of lattice preferred orientations. Within the materials science literature (e.g. Randle, 1992, 1993) the bulk texture, also called the *macrotexture*, of a polycrystal describes the volume fractions of particular orientations, i.e. without reference to particular grains or subgrains. A *microtexture*, on the other hand, is a texture of individual grains associated with one or more features of the microstructure. While the macrotexture and microtexture describe grain orientations, the *mesotexture* describes the 'texture between grains' or more specifically the lattice misorientation across grain boundaries.

We will use the following terms in this paper. The bulk lattice preferred orientation (or macrotexture) will be described by the term crystallographic preferred orientation (CPO). Microtextures will be described by reference to the type of grains measured, i.e. the CPO of large grains. The term grain misorientation distribution (MOD) will be used to describe the distribution of lattice misorientations across grain boundaries (i.e. the mesotexture). We will use these terms because the terms macro, meso and micro are commonly used in geology to specify the scale of observation.

2. Experimental techniques and methods

Electron back-scatter diffraction is a scanning electron microscopy technique which permits measurement of the full or complete orientation of

grains as small as 0.5 μm (Venables and Harland, 1973; Schwarzer, 1990; Gottstein, 1992; Randle, 1992, 1993). In SEM, orientation contrast imaging in Back-Scattered-Electron (BSE) mode is possible by mounting a solid-state back-scattered electron detector underneath the EBSD detector, i.e. in the forward-scattered position (cf. Reimer, 1985; Prior et al., 1996; Van der Wal and Dingley, 1996). In the resulting image the contrast is related to the orientation of the (sub)grain. By combining orientation contrast images with EBSD patterns the misorientation across all the grain and subgrain boundaries can be determined.

For EBSD analysis, the SEM sections were polished on a polyurethane lap for 3 h using a suspension of 0.05-μm silicon in water. It has been found that if the specimen is fine-grained (<50 μm) and tilted to 70º specimen drift is minimal and no coating was needed in the FEG SEM at 15–20 kV using beam currents around 0.5 nA (spot size 4–6). The lack of coating greatly improves pattern quality, since carbon coated specimens generally produce weaker EBSD patterns. Observations were taken a few millimetres away from the edge of the sample to reduce specimen charging.

EBSD patterns were indexed using the Channel^{+} package (Schmidt and Olesen, 1989). Since olivine possesses pseudo-hexagonal symmetry along the *a*-axis (Fig. 1) due to oxygen stacking (Poirier and Vergobbi, 1978), each solution has been rotated along the [*a*]-axes, to check the indexing. The error in the orientation determination is estimated at less than 1º (Schwarzer and Weiland, 1988; Schwarzer, 1990; Randle, 1992, 1993).

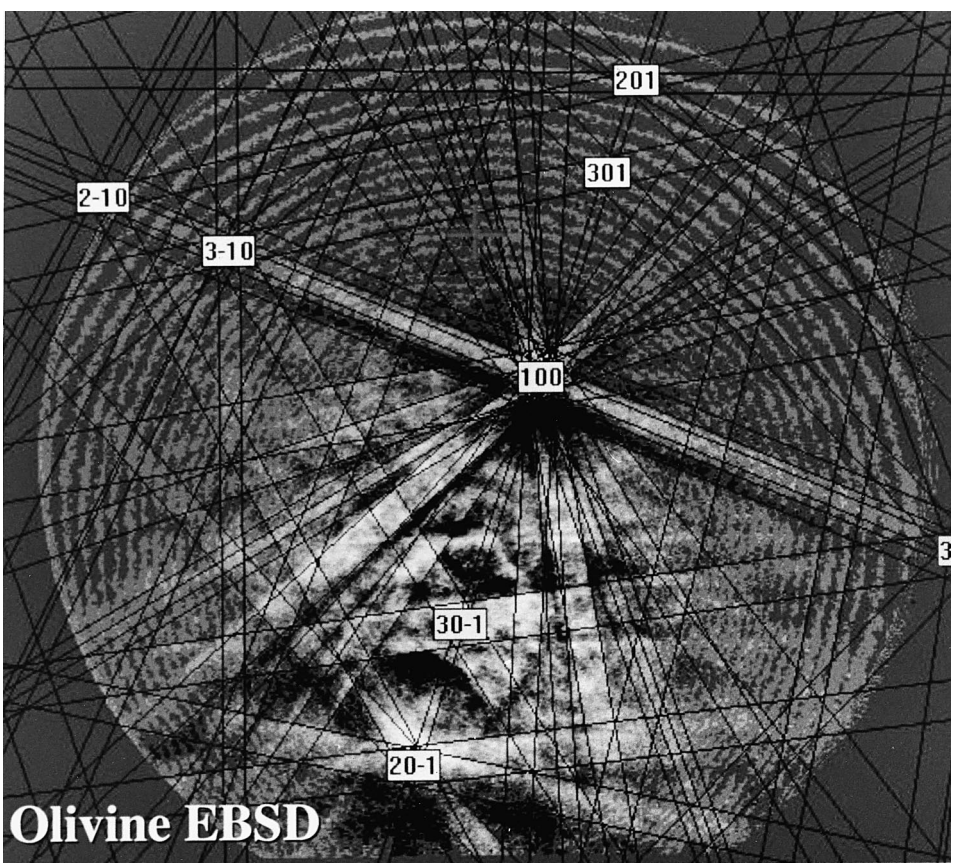

Fig. 1. Indexed electron back-scattered diffraction (EBSD) pattern from olivine showing the [100] zone axis. The strong diffraction bands that intersect the [100] axis produce pseudo-hexagonal symmetry which can cause problems with indexing if the weaker diffraction bands are not visible.

Orientation measurements have been used to establish the misorientation relationship between two adjacent grains and between subgrains. The misorientation between two grains can be described by an axis of rotation and a rotation about that axis (Randle and Ralph, 1986; Randle, 1992). The rotation axis is a direction which is common to both grains or subgrains about which the first must be rotated by the angle of misorientation in order to achieve the orientation of the second (Turner and Weiss, 1963; Randle and Ralph, 1986). An Excel™ spreadsheet has been written for the analysis of misorientation angles and axes in olivine. There are four equivalent ways of indexing each orthorhombic grain, and sixteen ways of expressing the misorientation (Grimmer, 1980). These misorientations occur in groups of four, with members of each group having the same angle of misorientation and rotation axes which are symmetrically equivalent. Consequently, a misorientation between two orthorhombic grains can be described in four different — but equivalent — ways, which in turn give four solutions of the axis/angle pair (Grimmer, 1980; Forwood and Clarebrough, 1991; Randle, 1993). Any of these four misorientations may be chosen as they are physically indistinguishable. Commonly, the axis/angle pair giving the smallest possible rotation is chosen as the misorientation (Randle and Ralph, 1986; Mainprice et al., 1993) and this is the approach adopted in this study. The rotation axes can be calculated both in crystal co-ordinates as well as in specimen co-ordinates. The latter approach can highlight specimen geometry effects, such as the relationships between rotation axes and the compression direction or sense of shear. As the accuracy in the CPO data is at maximum 1° (Schwarzer and Weiland, 1988: Schwarzer, 1990), it is assumed that the accuracy in misorientation angle is as good. This is in contrast to light-microscope techniques and TEM, where the accuracy in the CPO data is 2–5°, resulting in larger errors (5–20°) in the measured axis/angle pair of misorientation (see Avé Lallemant, 1985; Fliervoet and White, 1995). It should be noted that for small misorientations (generally $<2°$), this 1° error in orientation can result in large errors ($>10°$) in the orientation of the misorientation axis, whereas the error in the rotation angle is around 1° (Fliervoet and White, 1995).

Grain sizes have been measured from digitised line drawings of the orientation contrast images in SEM; using the public domain NIH Image program version 1.59 (developed at the US National Institutes of Health and available on the Internet at http://rsb.info.gov/nih-image/). The grain diameters were determined by taking the average of the long and short axis of each grain and were subsequently corrected for sectioning effects using a factor of 1.2 (cf. Underwood, 1970). As generally the grain sizes reveal a log normal distribution (Exner, 1972), the median (Md) of the distribution was taken as a measure of the grain size; half the inter-quartile range is taken as a measure of variability, the skewness (Sk) and kurtosis (Km) are given to characterise the spread of data around the median (Davis, 1986). Measurements of grain size using the linear intercept method in the light microscope have also been used to allow comparison with previous studies on olivine microstructures. We find that the grain size expressed as the median of the log-normal distribution obtained from processing of orientation contrast images is smaller than the mean grain diameter obtained from light microscopy.

The eigenvalues from the 'orientation tensor' have been used to evaluate the strength of a CPO (Woodcock, 1977; Davis, 1986). The eigenvalues have been calculated using the program Stereonet 4.9.6 (R.W. Allmendinger; public domain). The strength of a CPO is defined by:

$$C = \ln(S_1/S_3)$$

where S_1 and S_3 are the normalised eigenvalues of the CPO tensor. Uniform or random distributions will have a $C \approx 0$, strong CPOs have a larger C. The method assumes that the CPOs are unimodal clusters, axially symmetric girdles, or some combination of the two with (near) orthorhombic symmetry (Woodcock, 1977). Therefore, the eigenvalue method must be used with reference to the contoured CPOs.

3. Crystallographic preferred orientations and microstructures of experimentally deformed samples

There has been a vast amount of work on the deformation of olivine aggregates (Goetze, 1978;

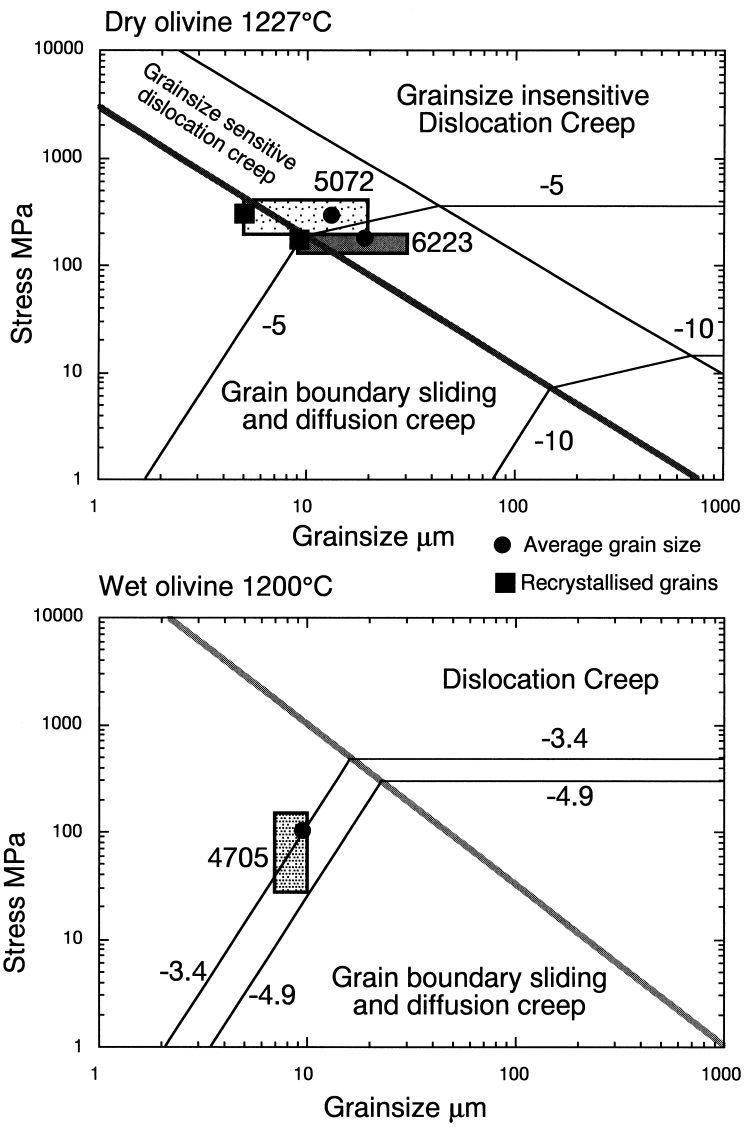

Fig. 2. Deformation mechanism maps for olivine. The shaded regions show the range of grain size and stress during the deformation experiment. The grain sizes shown are from light-microscopy measurements because the deformation mechanism maps have been calibrated using light-microscopy data on grain sizes. The dry olivine map is constructed for $T = 1227$ºC appropriate for sample 5072. Sample 6223 was deformed at 1300º and 1250ºC so the strain rate contours shown do not apply to that sample. The positions of the boundaries between the deformation regimes do apply approximately to sample 6223 because the positions of these boundaries are relatively insensitive to temperature (Drury and Fitz Gerald, 1998). The maps show that samples 5072 and 6223 were deformed in the grain-size-sensitive dislocation creep regime with the small recrystallised grains close to the transition to diffusion creep. Sample 4705 was deformed well into the diffusion creep regime.

Karato and Wu, 1993; Drury and Fitz Gerald, 1998). Three different deformation regimes have been identified. Two regimes, dislocation creep and diffusion creep have been known for some time (Karato et al., 1986) (Fig. 2). In the literature on olivine deformation the term ‘diffusion creep’ is used to describe grain-size-sensitive creep with the strain rate proportional to σ^n and d^{-m}, where $n = 1$–2 and $m = 2$–3.

Table 1
Deformation conditions of samples described in this study

Sample	Reference	Temp. (ºC)	Flow stress (MPa)	Strain rate (s^{-1})	Final strain (%)	Stress exponent	Grain size SEM (μm)	Grain size light micr.
4705	Chopra (1986)	1200	150	1.5×10^{-4}			5.0±1.9	
		1200	28	1.4×10^{-5}		0.7	(1–12)	9.5 μm
		1200	105	4.3×10^{-4}	24.0	1.2		
5072	Hitchings et al. (1989)	1227	190	1.3×10^{-5}				mean 13 μm
		1227	310	4.5×10^{-5}		2.7	2.4±1.0	
		1227	405	1.3×10^{-4}		3.8	(0.5–12)	
		1227	295	4.8×10^{-5}	19.8			recryst. 5 μm
6223	Drury (1992, unpubl.)	1300	130	3.6×10^{-5}	6.5	3.3	9.2±3.0	mean 19 μm
		1250	181	3.1×10^{-5}	8.6		(2–30)	recryst. 7 μm
DR 89.3	Van der Wal (1993)		≈30					≈170 μm
Dreiser	Avé Lallemant (1985)		≈1–10					1–5 mm

The relative roles of grain boundary sliding and diffusion in this regime are not known in detail. Recently, for dry olivine two different types of dislocation creep have been identified (Hirth and Kohlstedt, 1995; Drury and Fitz Gerald, 1998), one in which the strain rate is independent of grain size and the strength is controlled by the strongest slip system, and a second regime where deformation is accommodated by a combination of glide on the weakest slip system and grain boundary sliding (Hirth and Kohlstedt, 1995). A similar regime probably occurs in wet olivine (Chopra, 1986). We have chosen three different samples for our study on the variation of CPO and grain boundary MOD with deformation conditions. The experimental conditions are listed in Table 1 and shown on a deformation mechanism map in Fig. 2. The samples selected include two specimens from the grain-size-sensitive dislocation creep regime and one sample from the diffusion creep regime. We have selected samples from the grain-size-sensitive dislocation creep regime because this regime will be important whenever dynamic recrystallisation controls the grain size of olivine rocks (Drury and Fitz Gerald, 1998). All samples were deformed in Paterson gas-medium apparatus at the Research School of Earth Sciences of the Australian National University. Deformation tests were run at 300 MPa confining pressure with the oxygen fugacity limited by the iron jackets. All samples were synthetic olivine rocks made from hot-pressed natural olivine (Fo_{91}) powders (Chopra, 1986; Hitchings et al., 1989; Drury, unpublished work, 1992). The initial CPO in hot-pressed olivine samples is weak to random (Karato, 1988).

3.1. Diffusion creep sample (4705)

Sample 4705 (Chopra, 1986) was deformed to 24% strain with added water at 1473 K and underwent three deformation steps (150, 28 and 105 MPa). The stress exponent n is close to unity (0.7–1.2). The olivine grain size (Fig. 3a) is small at 5.0 ± 1.9 μm (Sk: 1.0; Km: 1.0) and fairly uniform (ranging from 1 to 12 μm). This average grain size is roughly equal to, to slightly smaller than the size of the very few (5%) subgrains encountered in the larger grains. Although there is a slight elongation of the grains, the direction of the elongation does not have a strong preferred orientation (Fig. 5). The olivine grains are equiaxed with straight to curved grain boundaries, resulting in a polygonal microstructure (Fig. 3a). A mean grain diameter of 9.5 μm was obtained by light-microscopy measurements (Chopra, 1986).

The CPO (Fig. 6a) is fairly uniform for the [a]-, [b]- and [c]-directions ($C \approx 0.3$–0.4). There are minor, weak maxima of [b]-axes parallel to the compression direction, and of [c]-axes perpendicular to the compression direction at the edge of the pole figure. Low-pole density areas are essentially absent to limited.

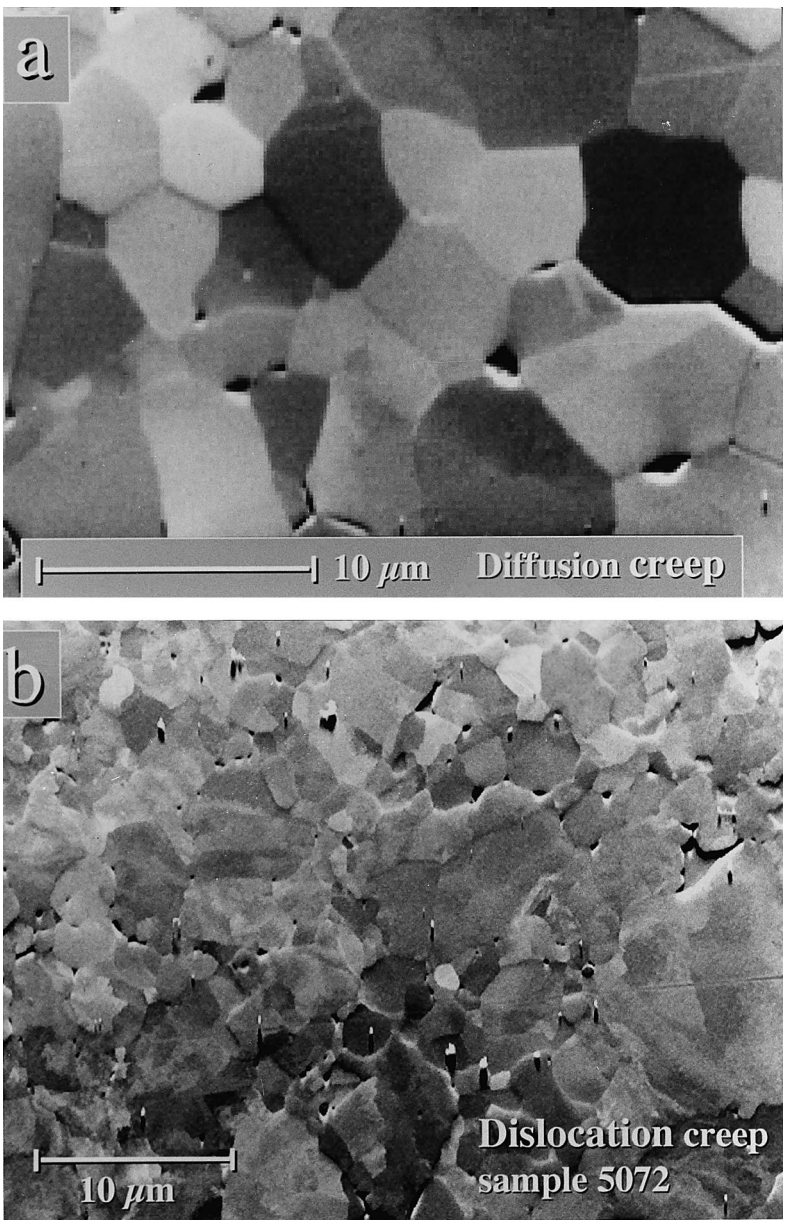

Fig. 3. Orientation contrast, forward-scattered, SEM images of experimentally deformed olivine rocks with the compression axis horizontal. (a) Polygonal, equant, grain microstructure in sample 4705 deformed by diffusion creep. Larger grains contain subgrains. Voids occur along grain boundaries and at triple points. (b) Microstructure of sample 5072 deformed by dislocation creep. Large old grains are surrounded by smaller subgrains and recrystallised grains. Note that many grain boundaries are indistinct in this image.

3.2. Dislocation creep sample 1 (5072)

Sample 5072 (Hitchings et al., 1989) was deformed at 1227 K with no added water. The stress exponent is close to 3. The total strain is around 20% and the stresses varied between 190 and 405 MPa. The microstructure (Figs. 3b and 4a) consists of large grains surrounded by numerous smaller grains. The grain size is very small at 2.4 ± 1.0 μm (Sk: 2.1; Km: 5.0) but not uniform ranging from 0.5 to 12 μm.

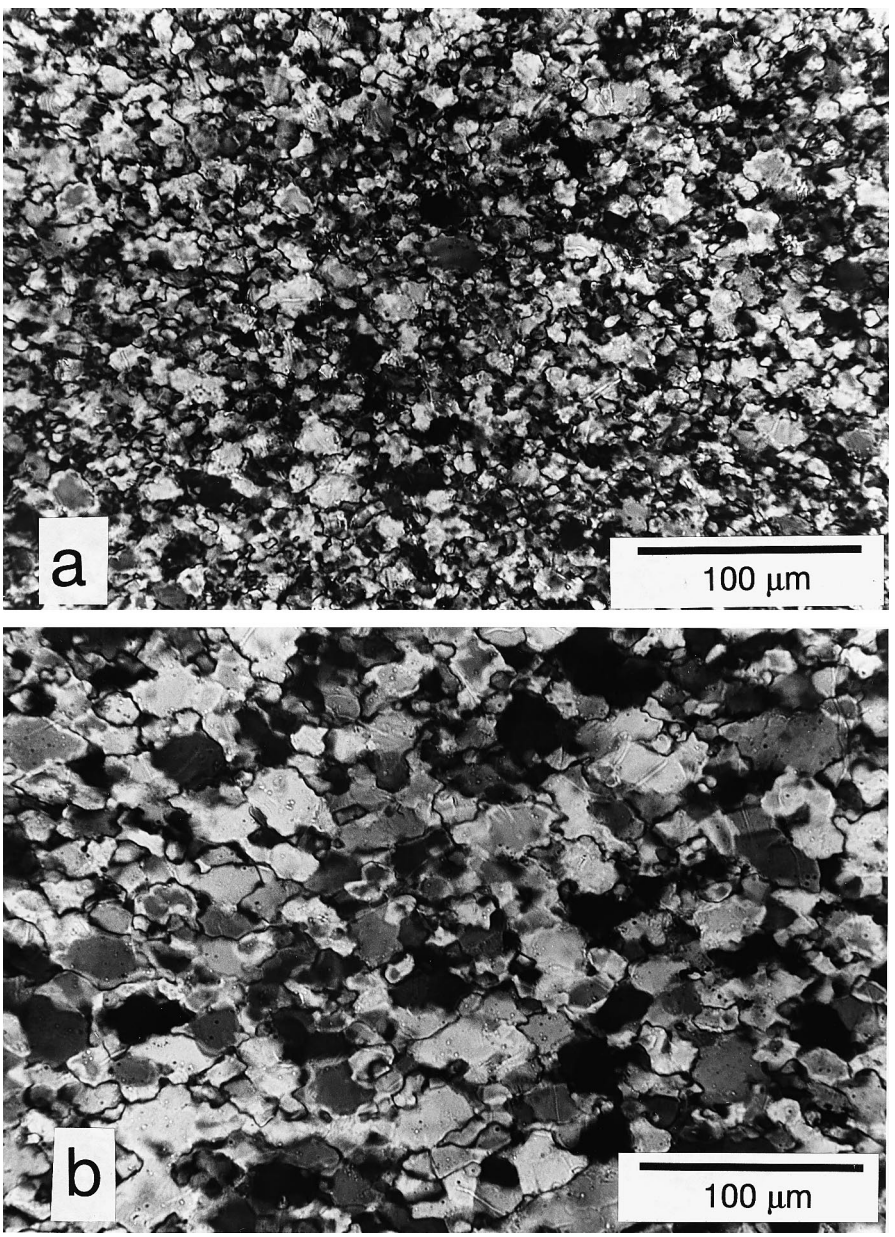

Fig. 4. Transmitted polarised light images of experimentally deformed olivine samples. (a) Sample 5072 deformed by dislocation creep showing bimodal microstructure with large old grains surrounded by smaller recrystallised grains. (b) Sample 6223 deformed by dislocation creep at lower stress than sample 5072, showing similar but coarser-grained microstructure than (a). Note that in (b) the grain boundaries have a tendency to be aligned at angles of $\pm 45^{o}$ to the compression axis.

This latter value is greatly influenced by the magnification since many of the larger grains are truncated at the edge of the micrograph. The mean grain size calculated from linear intercept measurements in the light microscope is 13 μm with a recrystallised grain size around 5 μm. Grains up to 30 μm have been observed in the light microscope (Fig. 4a). These large grains show undulatory extinction and have subgrains roughly 2–5 μm in size. The grains are elongated with a preferred orientation of elongation

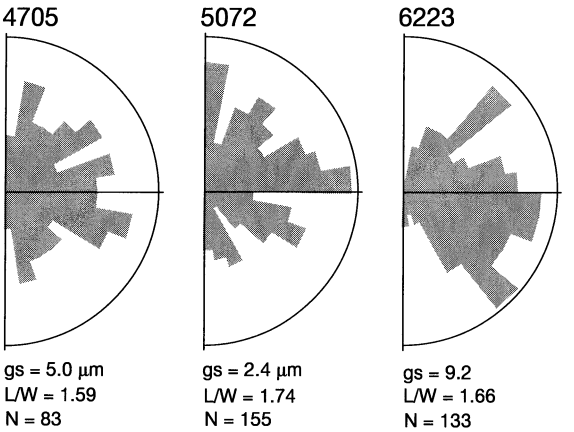

Fig. 5. Rose diagrams showing the orientation distribution of the long axis of olivine grains as measured within the experimental samples (gs = grain size, L/W = ratio of long and short axis, N = number of measurements; full circle = 10%).

directions into several maxima (Fig. 5). Two of the maxima are symmetrically arranged at angles of 45° to the compression direction, one perpendicular to the compression axis, and one parallel to it. Grain boundaries are generally curved and serrated suggesting grain boundary migration had occurred. The shapes of the large grains are very irregular, whereas the smaller grains are more polygonal.

Although not strong, the CPO in this sample (Fig. 6b) is stronger than that of sample 4705 ($C \approx 0.5$–0.7). The strength of the CPO is most clearly seen in the [b]-axis pole figure where a strong maximum has developed sub parallel to the compression direction ($C = 0.7$). The [a]-axes define a girdle perpendicular to the compression axis. The CPO of the small number of large grains measured is stronger ($C = 0.7$–1.4) than the CPO of small grains ($C = 0.5$–0.7) (Fig. 7a,b).

3.3. Dislocation creep sample 2 (6223)

Sample 6223 (Drury, unpublished work, 1992) underwent a complex history. It was first deformed at 1573 K to 6.5% strain with a final stress of 130 MPa. After two annealing stages at 1573 K for 30 min and at 1523 K for 30 min, the sample was deformed to another 8.6% strain with a final stress of 181 MPa. The deformation history was ended by a 1-h stress relaxation test at 1553 K in which another 1.9% strain accumulated with a final stress of 57 MPa. The stress exponent determined from the relaxation test is between 3 to 4. The total strain was 17%.

The olivine grain size (Fig. 4b) is small at 9.2 ± 3.0 μm (Sk: 1.6; Km: 2.3) but not uniform (ranging from 2 to 30 μm). The microstructure consists of several large grains surrounded by numerous smaller grains. These large grains have subgrains roughly 5 μm in size. The grains are elongated with a preferred orientation of elongation directions at ±45° to the compression direction (Fig. 5). The mean grain size estimated from linear intercepts in the light microscope is 19 μm with a recrystallised grain size of 7 μm. Grain boundaries are curved and serrated suggesting grain boundary migration had occurred. The larger grains have a diamond shape (Drury and Fitz Gerald, 1998) (Fig. 4b) and commonly show undulatory extinction. Grain boundaries between large grains are irregular in shape.

The CPO (Fig. 6c) is weaker than in the dislocation creep sample 5072 but stronger than the diffusion creep sample 4705 ($C \approx 0.4$–0.5). The [a]-axes define a broad girdle perpendicular to compression axis, whereas a low density area of [b]-axes occurs in the centre of the pole figure. A higher density area occurs in the [c]-axis pole figure parallel to the compression axis. There is little difference in the strength of the CPO between large and small grains (Fig. 7c,d). Besides the weaker CPO and the diamond shape of the larger grains, this sample 6223 has a very similar microstructure (Fig. 4b) to the dislocation creep sample 5072 (Fig. 4a).

4. Grain misorientation distributions

Grain misorientation distributions can be described either by the misorientation distribution function (MODF) in Euler space (e.g. Mainprice et al., 1993) or by the distribution of axis–angle data. Misorientation angle–axis data can be represented in full using Rodrigues–Frank space (Randle, 1993) or misorientation space (e.g. Lloyd et al., 1997). All of these methods result in a three-dimensional plot which can only be presented easily in terms of projections or sections. The most straightforward way to present the data is on sections of misori-

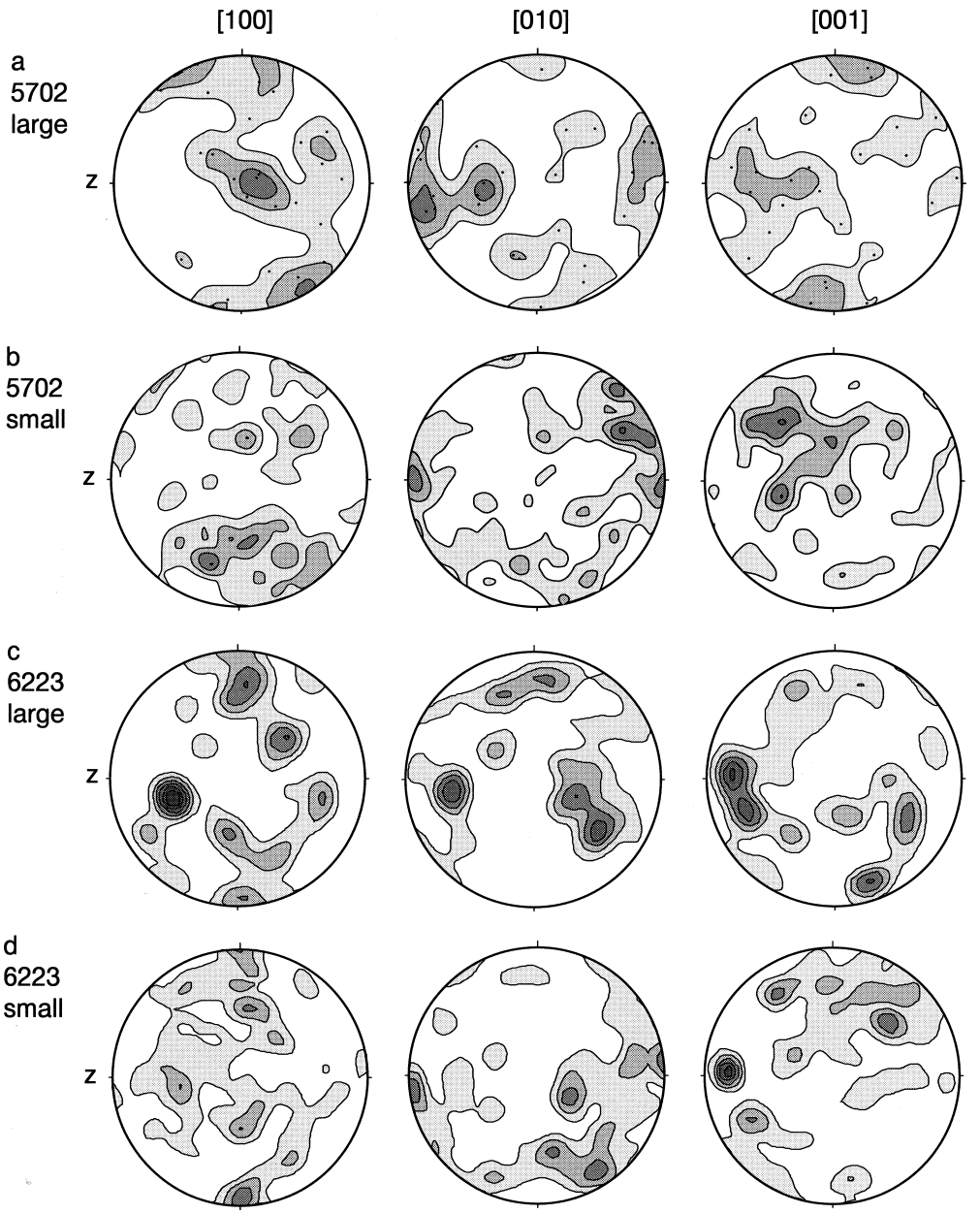

Fig. 7. Pole figures showing the difference in crystallographic preferred orientation of large and small grains in (a, b) sample 5072 and (c, d) sample 6223. Contour intervals are drawn at 2σ (Kamb's method), the compression direction is horizontal, $N = 29$ (a), 193 (b), 65 (c), 134 (d).

Fig. 6. Pole figures showing the crystallographic preferred orientations: (a–c) experimental samples, (d–e) natural samples. Contour intervals drawn at 2σ (Kamb's method), in (a–c) the compression direction (z) is horizontal, in (d–e) S is the pole to the foliation and L the lineation. (a) Diffusion creep sample showing a very weak texture, $N = 198$. (b) Dislocation creep sample (5072) showing a maximum of [b]-axes parallel to the compression axes. $N = 225$. (c) Dislocation creep sample showing a broad girdle of [a]-axes perpendicular to the main compression direction $N = 199$. (d) Strong CPO of the garnet mylonite $N = 116$. (e) Strong CPO of Dreiser Weiher nodule $N = 53$ (modified after Avé Lallemant, 1985).

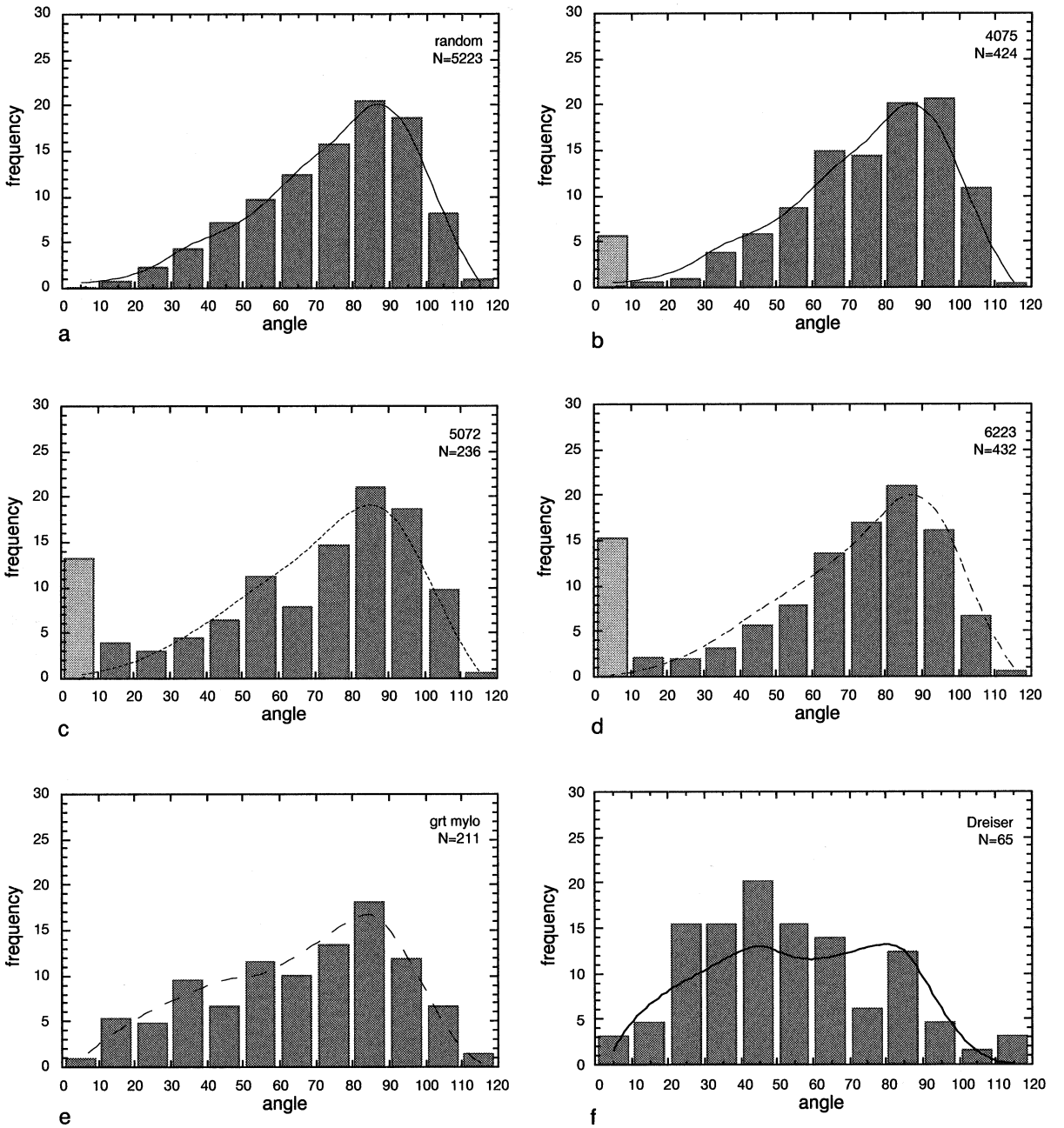

Fig. 8. Distribution of misorientation angles between adjacent olivine grains. Misorientations below 10° are designated as subgrains and are shown in a brighter tone. In each histogram, the associated uncorrelated MOD is shown as a thin line (see text for discussion). In assuming that the CPO of 4705 is random, the histogram in (a) shows the distribution of angles for a statistically random case (see text for discussion).

entation space which display the misorientation axis distribution associated with a particular range of misorientation angles. The misorientation space sections are presented both as inverse pole figures and stereonets showing the distribution of axes with respect to the specimen reference frame. We have also pre-

sented the data by misorientation angle distributions (MAD) displayed as a histogram because these plots are useful in the assessment of the frequency of different types of grain boundary (subgrain boundaries, general boundaries, special boundaries).

The first step in the analysis of misorientation distributions is to establish which misorientations are possible and the probability of their occurrence. The probability of individual misorientations is determined by the nature and strength of the CPO. Very strong CPOs produce more low to intermediate-angle misorientations, whereas weaker CPOs produce misorientations closer to a random distribution. The misorientation probabilities imposed from the CPO (most commonly termed the uncorrelated misorientation distribution (Randle, 1992; Mainprice et al., 1993) can be characterised in several ways (Randle, 1993; Lloyd et al., 1997). We have obtained the uncorrelated misorientation distributions by taking around 5000 randomly selected grain pairs and calculating their associated misorientation. The grain pairs include adjacent grains and grains not in physical contact. This approach is similar to the method of factorial misorientation analysis described by (Lloyd et al., 1997). As sample 4705 is essentially random we have used the uncorrelated misorientation distributions obtained from this sample to represent the random distribution. The distribution of misorientation angles obtained (Fig. 8a) is a strongly skewed distribution with a peak at 90° and a maximum angle of 117°. A similar random distribution has been calculated by Faul and Fitz Gerald (1999). The restricted range of misorientation axis and angle arises from the fact that rotations greater than 120° can always be described by a smaller angle rotation around a different axis (Grimmer, 1980).

The observed misorientations (obtained from nearest neighbour analysis, Lloyd et al., 1997) should be compared with the uncorrelated misorientation distribution to determine if 'significant misorientations' occur. Significant misorientations may arise either because certain misorientations have a low-energy boundary structure (McLaren, 1986) or because particular deformation or recrystallisation processes produce characteristic boundary types (e.g. twinning, or subgrain rotation recrystallisation). In the comparison between uncorrelated and correlated MOD, boundaries below 10° are considered to be

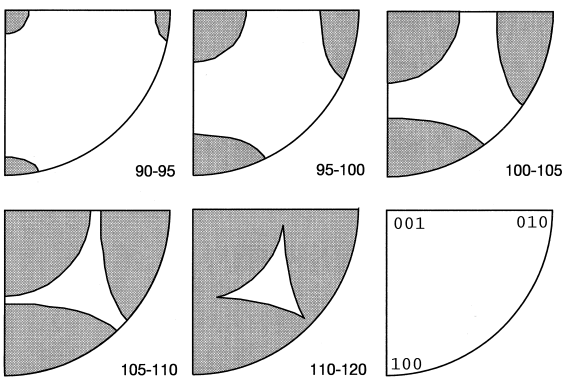

Fig. 9. Inverse pole figures showing the forbidden misorientation axes (shaded areas) at high misorientation-angles.

subgrain boundaries (cf. White, 1976; Buatier et al., 1991) and are omitted in the comparison. The uncorrelated misorientation axis distributions have been characterised and for all cases show a random distribution over all misorientation angles. Chi-squared (χ^2) tests have been performed when comparing the MADs. At 10% significance, the critical value of χ^2 is 12.0 at 7 degrees of freedom. The degrees of freedom are taken as the number of categories in the histogram minus 3 (Davis, 1986). As there are generally very few boundaries having angles $>110°$, these are grouped with those of $>100°$. The comparison between observed and uncorrelated misorientation axis distributions has been made using inverse pole figures or sections of misorientation space.

In the forthcoming sections, the data-sets have been divided into four subsets: subgrain boundaries, 0–10°; intermediate-angle boundaries, 10–60°; high-angle boundaries 60–90°; and very high-angle boundaries from 90° to the maximum angle of 117°. Up to a misorientation angle of 90° the axes of misorientation can occupy the entire unit triangle (cf. Grimmer, 1980). At high rotation angles, however, certain misorientation axes are forbidden (Fig. 9). Therefore, in the inverse pole figure displaying the axes/angle pairs with very high angles ($>90°$), a 'natural' maximum of axes occurs in the centre of the pole figure, i.e. near [121] (Fig. 9).

4.1. Diffusion creep sample (4705)

The distribution of misorientation angles between adjacent grains (Fig. 8b) in sample 4705 (diffusion

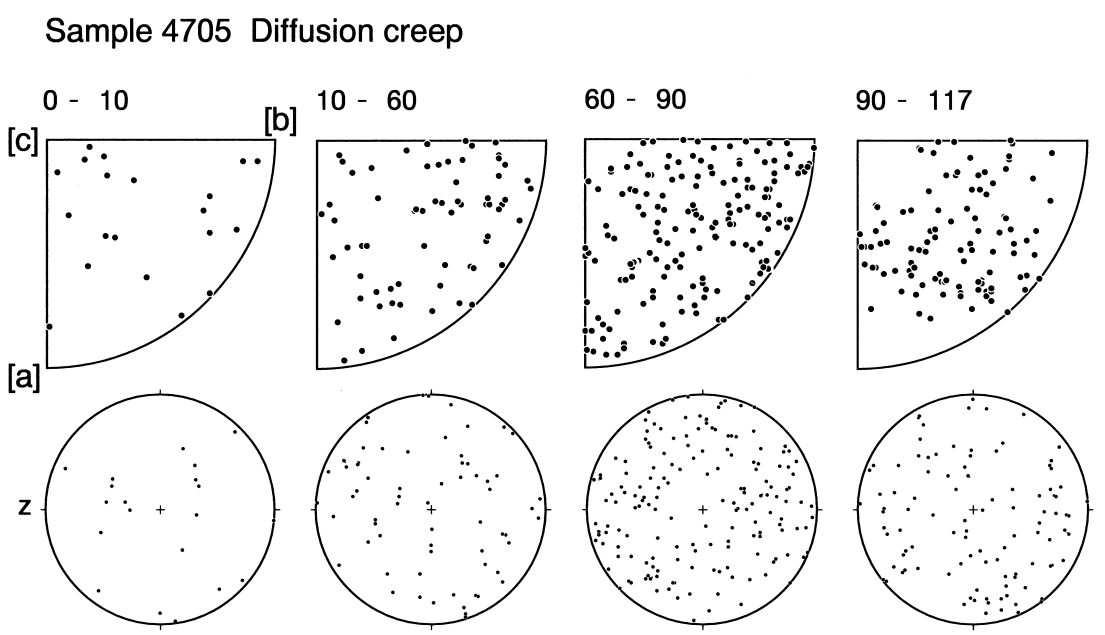

Fig. 10. Misorientation distribution analysis of sample 4705. Misorientation axes are plotted in inverse pole figures in the upper row and with respect to the specimen reference frame in the lower row of stereonets, with z the compression axis, horizontal. The misorientation axes show no obvious preferred orientations.

creep) resembles its uncorrelated MOD (Fig. 8a) with a $\chi^2 = 9.3$. As noted above this is the statistically random case (Fig. 8a). There is no strong preferred orientation of the misorientation axes between adjacent grains, either in terms of crystal co-ordinates or expressed in specimen co-ordinates (Fig. 10). Only the axes of misorientation between adjacent subgrains show a tendency to plot away from the [a]-axis.

4.2. Dislocation creep sample 1 (5072)

The distribution of angles of misorientation in sample 5072 (Fig. 8c) deviates from its uncorrelated MOD (Fig. 8c), with $\chi^2 = 22.5$. However, the shape of the observed MOD still follows that of the uncorrelated MOD (Fig. 8c). All of the difference is accounted for by the higher frequency of boundaries with misorientations between 10 and 20°, and to a lesser extent to the lower frequency of boundaries with a mismatch between 60 and 70°. The distribution of misorientation axes shows no obvious preferred orientation either in terms of specimen or crystal co-ordinates (Fig. 11). Misorientation axes between adjacent subgrains show a tendency to plot away from the [a]-axis.

This sample has a 'bi-modal' microstructure with 'large' (>5 μm) and 'small' (<5 μm) grains. Using this subdivision, the distribution of misorientation angles between large and small grains have been calculated (Fig. 12). The observed MOD clearly deviates from its associated uncorrelated MOD ($\chi^2 = 40.8$). There are many boundaries with misorientation angles between 10 and 20° and between 40 and 50°, and few with angles between 60 and 80° (Fig. 12). At high angles the mode of the distribution is shifted towards 90–100°. The misorientation axes between these large and small grains have been divided into two sets and plotted in crystal co-ordinates (Fig. 12). Care should be taken with such a procedure as relatively few boundaries are encountered. The misorientation axes corresponding to high-angle (>90°) boundaries plot away from the [c]-axis, whereas those corresponding to lower-angle boundaries tend to be at a high angle to [b]. However, those with a mismatch <20° plot near the [c]-axis. These distributions are clearly different from the uncorrelated misorientation axis distribution which has a random distribution.

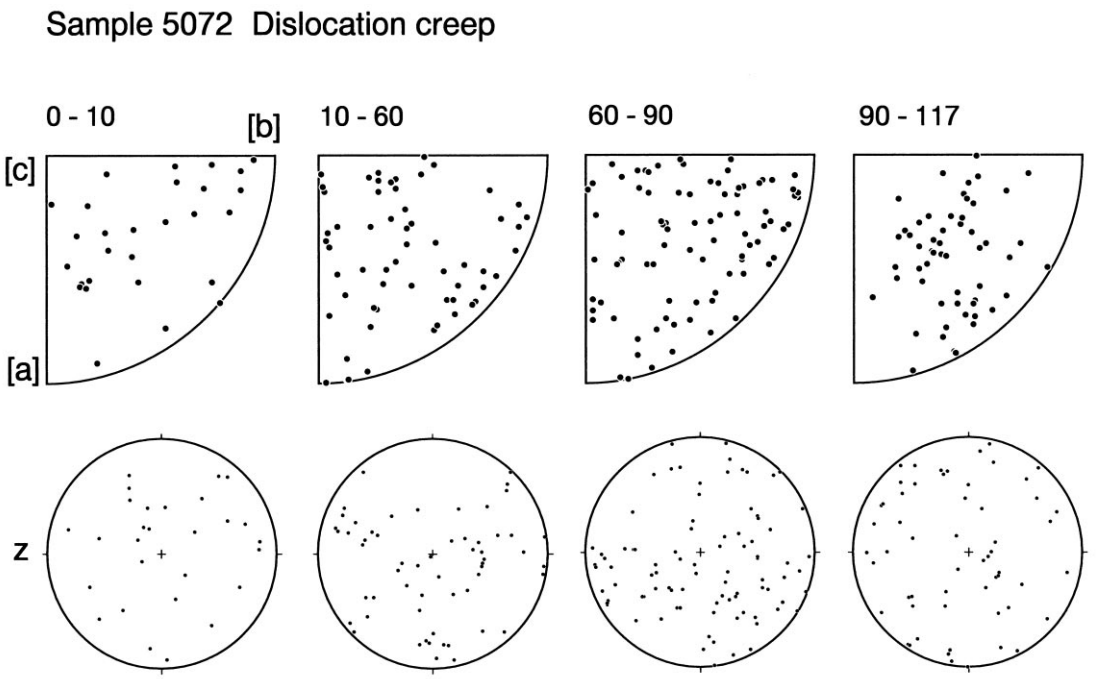

Fig. 11. Misorientation distribution analysis of sample 5072. Misorientation axes are plotted in inverse pole figures in the upper row and with respect to the specimen reference frame in the lower row of stereonets, with *z* the compression axis, horizontal. The misorientation axes show no obvious preferred orientation.

The misorientation angles between small grains (Fig. 12) more closely follow the uncorrelated MOD ($\chi^2 = 11.4$). Too few boundaries between adjacent large grains were encountered in the sample. There is no obvious preferred orientation of misorientation axes between small grains, either in terms of crystal co-ordinates or in specimen co-ordinates (Fig. 12).

4.3. Dislocation creep sample 2 (6223)

Besides the numerous subgrains encountered in the sample, the distribution of misorientation angles between adjacent grains of sample 6223 follows that of its uncorrelated MOD (Fig. 8d), with $\chi^2 = 7.1$. Moreover, the axes of misorientation as described in both specimen and crystal co-ordinates show no obvious preferred orientation (Fig. 13). As in sample 5072, this sample consists of several large grains surrounded by smaller grains. The distribution of angles between 'large' grains (>10 μm) clearly differs from the uncorrelated MOD in that low and intermediate angles are absent, whereas boundaries with high angles occur more frequently compared to the uncorrelated MOD (Fig. 14). The distribution of mismatch angles between small grains (<10 μm) follows that of the uncorrelated MOD ($\chi^2 = 8.1$) (Fig. 14). However, there is a shift of the mode of the distribution to 70–90°. The distribution of misorientation angles between small and large grains is similar to the uncorrelated MOD, but deviates in detail ($\chi^2 = 21.3$) (Fig. 14). There are somewhat more low- to intermediate-angle boundaries (10–20°), the mode of the distribution is displaced towards 90–100° and there are fewer boundaries with a 50–60° mismatch. The axes of misorientation show no preferred orientation (Fig. 14), either in crystal co-ordinates, or in the specimen reference frame.

5. CPO and grain MOD's in some naturally deformed olivine rocks

It is apparent that in the experimental samples the observed MOD largely follows the uncorrelated

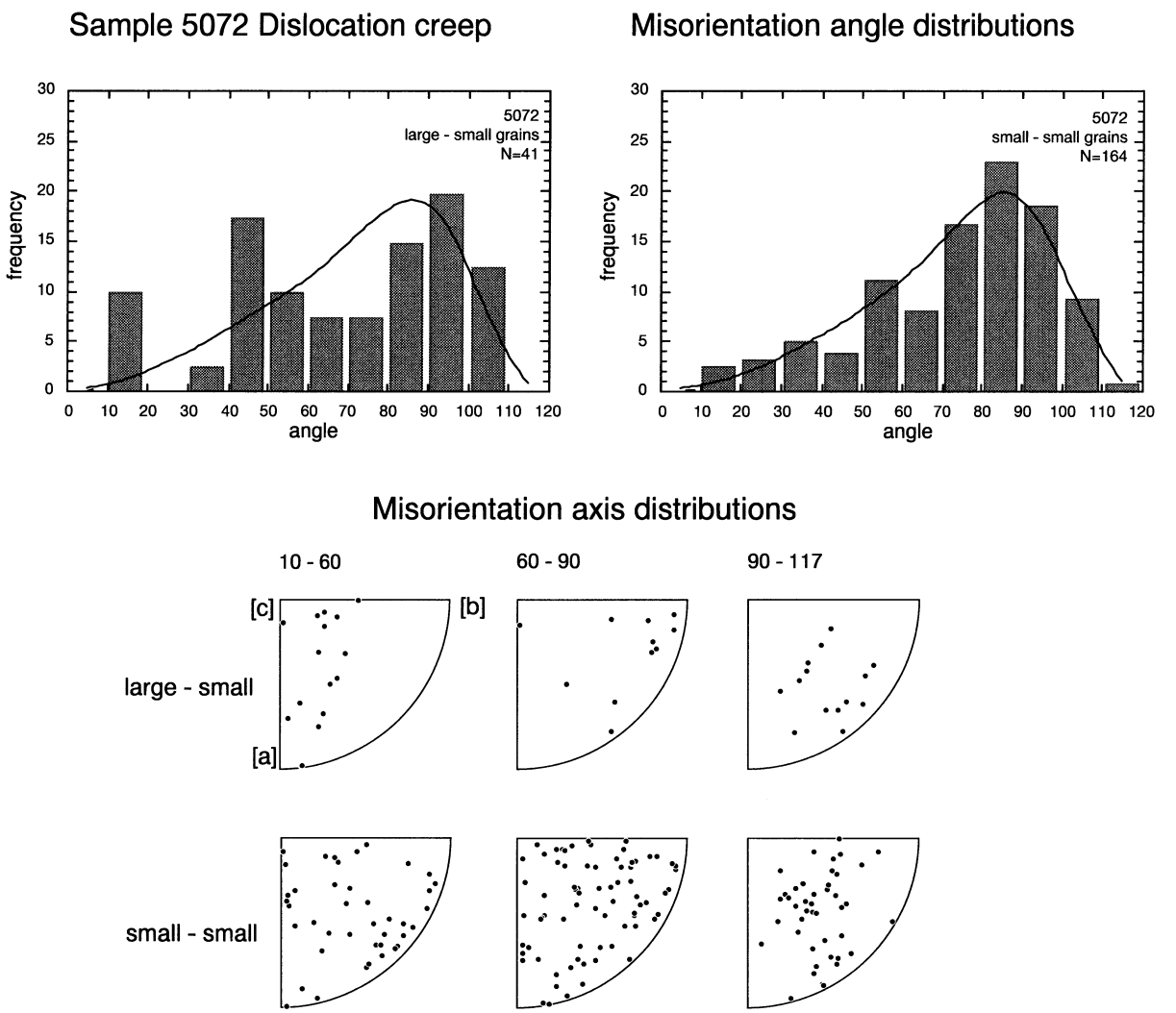

Fig. 12. Misorientation distribution analysis of sample 5072 with a subdivision on grain size. Histograms show the misorientation angle distributions. In each histogram, the associated uncorrelated MOD is shown as a thin line. The MOD between large and small grains clearly differs from that between small grains (see text for discussion).

MOD and only small differences exist between the two. In samples 5072 and 6223 the frequency of low- to intermediate-angle boundaries ($<20^{o}$) is slightly higher than expected. For 5072 the frequency of 60–70° boundaries is somewhat elevated. In all samples, the axes of misorientation between adjacent subgrains show a tendency to be at a high angle to the [*a*]-axis. The largest differences occur within the MOD's of the separate microstructural domains (or subsets) (Figs. 12 and 14).

It is important to note, however, that all of the experimental samples were deformed only to low or moderate strain of 17–24%. The CPO in the experimental samples are not as strong ($C \approx 0.3$–1.0) as in many naturally deformed olivine rocks ($C > 1$). In this section we describe the CPO and MOD's of two naturally deformed olivine rocks: a garnet-spinel mylonite (DR 89.3) from the Ronda peridotite (Van der Wal, 1993) and a lherzolite xenolith from Dreiser Weiher, Germany (Avé Lallemant, 1985).

Garnet mylonite. The microstructure is characterised by elongate olivines and minor pyroxene

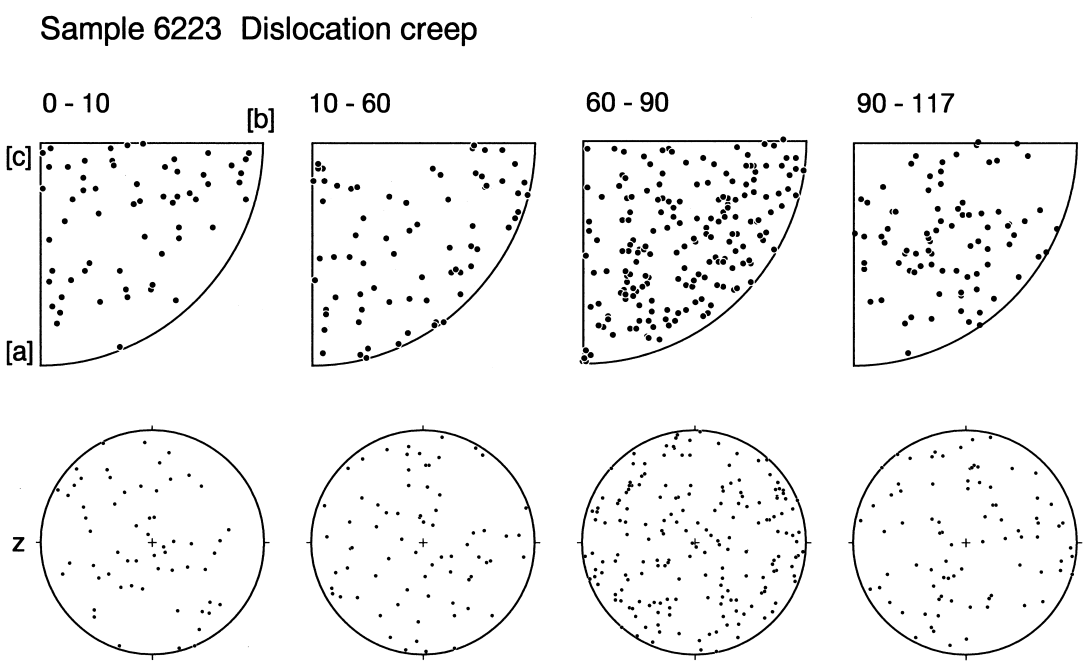

Fig. 13. Misorientation distribution analysis of sample 6223. Misorientation axes are plotted in inverse pole figures in the upper row and with respect to the specimen reference frame in the lower row of stereonets, with z the compression axis, horizontal. The misorientation axes show no obvious preferred orientation.

grains aligned parallel to the foliation. The olivine grain size is heterogeneous with a few relict grains (0.5–1 mm) in a matrix of smaller recrystallised grains (25–200 μm). The olivine texture (Fig. 6d) is strong ($C \approx 0.8$–1.6) (Van der Wal, 1993). The olivine [a]-axes are concentrated in a dominant maximum sub-parallel to the lineation, with a partial girdle sub-parallel to the foliation plane and a second maximum in the centre of the pole figure. The [b]-axes are mainly concentrated in a point maximum perpendicular to the foliation. The olivine [c]-axes are concentrated in a point maximum in the centre of the pole figure. The large grains have orientations similar to the small grains. As argued by Van der Wal (1993), these CPOs suggest that deformation occurred dominantly by dislocation creep processes involving slip on the [100] (010) slip system.

The distribution of misorientation angles between adjacent grains is shown in Fig. 8e. In general the observed distribution follows its associated uncorrelated MOD ($\chi^2 = 10.4$). It should be noted that the shape of the uncorrelated MOD differs significantly from a random MOD, in that boundaries with low to intermediate misorientations have a higher frequency. The misorientation axes show some preferred orientation (Fig. 15a). Those corresponding with intermediate misoriented boundaries (10–60°) tend to be concentrated perpendicular to [a], while those associated with higher mismatch (60–90°) tend to be more perpendicular to [c].

The distribution of angles between 'large' and 'small' grains differs from its associated uncorrelated MOD with a high frequency of 20–40° boundaries (Fig. 15b). The misorientation axes between grains with intermediate mismatch angles (10–60°) show a clear preference to be perpendicular to the [a]-axis (Fig. 15c). Those associated with higher mismatches tend to be perpendicular to [c]. The distribution of mismatch angles between small grains follows that of the uncorrelated MOD ($\chi^2 = 10.9$) (Fig. 15b). There is no obvious preferred orientation of misorientation axes between small grains in crystal co-ordinates (Fig. 15c).

Dreiser Weiher nodule. The data have been taken from (Avé Lallemant, 1985). This nodule is completely recrystallised with a grain size of about 1

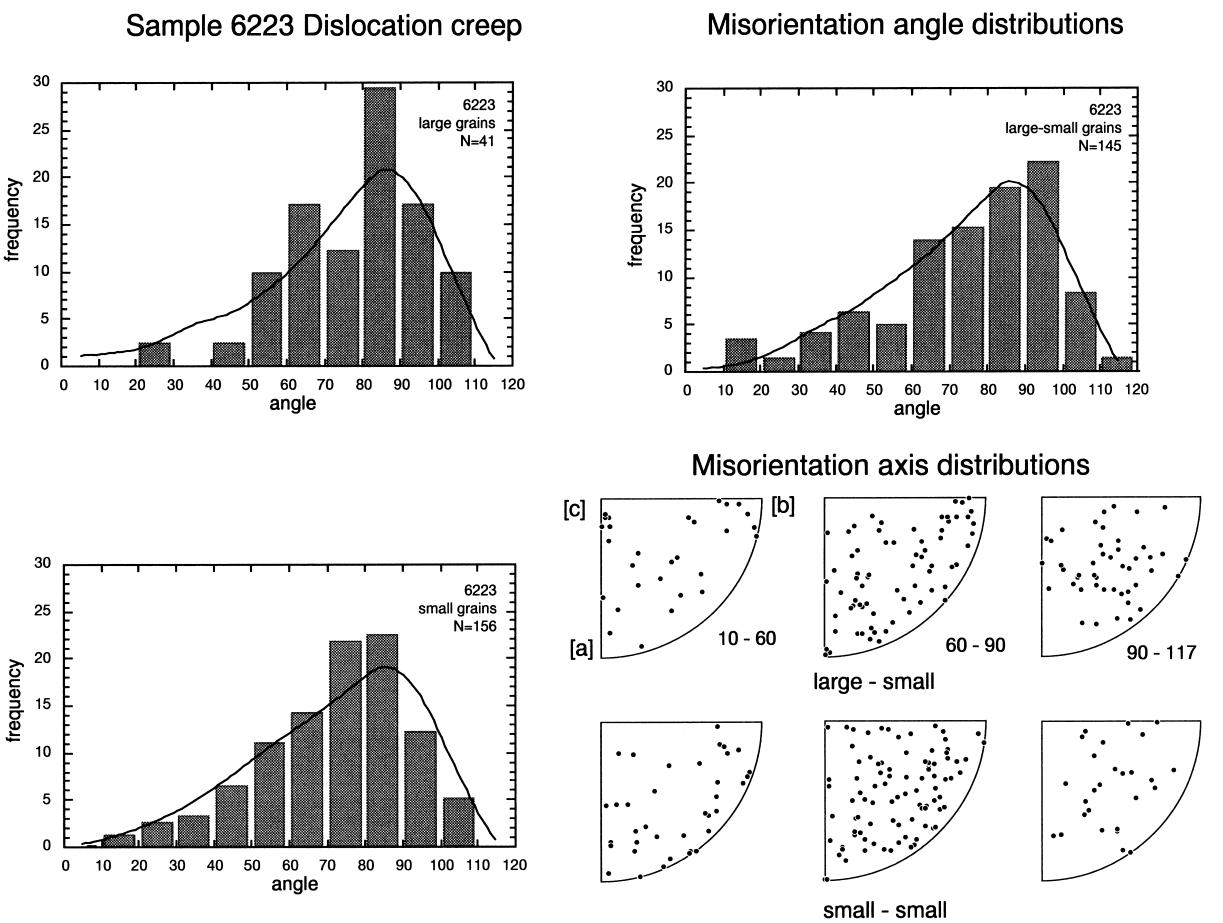

Fig. 14. Misorientation distribution analysis of sample 6223 with a subdivision on grain size. Histograms show the misorientation angle distributions. In each histogram, the associated uncorrelated MOD is shown as a thin line. The MOD between large grains clearly differs from the MOD between small grains and the MOD between large and small grains. The MOD between large and small grains is similar to the MOD between small grains (see text for discussion).

mm. The grains have a large aspect ratio and are tabular parallel to (010). Most olivines show planar subgrains elongated subparallel to (010). The olivine texture is strong ($C \approx 1.0$–2.9) with the olivine [b]-axes concentrated perpendicular to the grain elongation. Olivine [a]-axes define a girdle with a maximum parallel to the grain elongation. Olivine [c]-axes are (weakly) concentrated in a point maximum in the centre of the pole figure. The CPO suggests that deformation occurred dominantly by dislocation creep processes on the [a] (010) slip system. The misorientation angle distribution is shown in Fig. 8f. The misorientation axes are close to the [b]-axes (Avé Lallemant, 1985).

Fig. 15. (a) Misorientation axis distribution analysis of naturally deformed olivine mylonite (DR89.3). Note that for intermediate-angle (10–60º) boundaries, there is a tendency for many misorientation axes to be aligned away from the [a]-axis. (b) Misorientation angle distributions of (DR89.3) with a subdivision on grain size. In each histogram, the associated uncorrelated MOD is shown as a thin line. Although the two MOD's clearly differ, they tend to follow the associated uncorrelated MOD. (c) Misorientation axes distributions for sample DR98.3. The axes for intermediate-angle boundaries show a tendency to be perpendicular to [a].

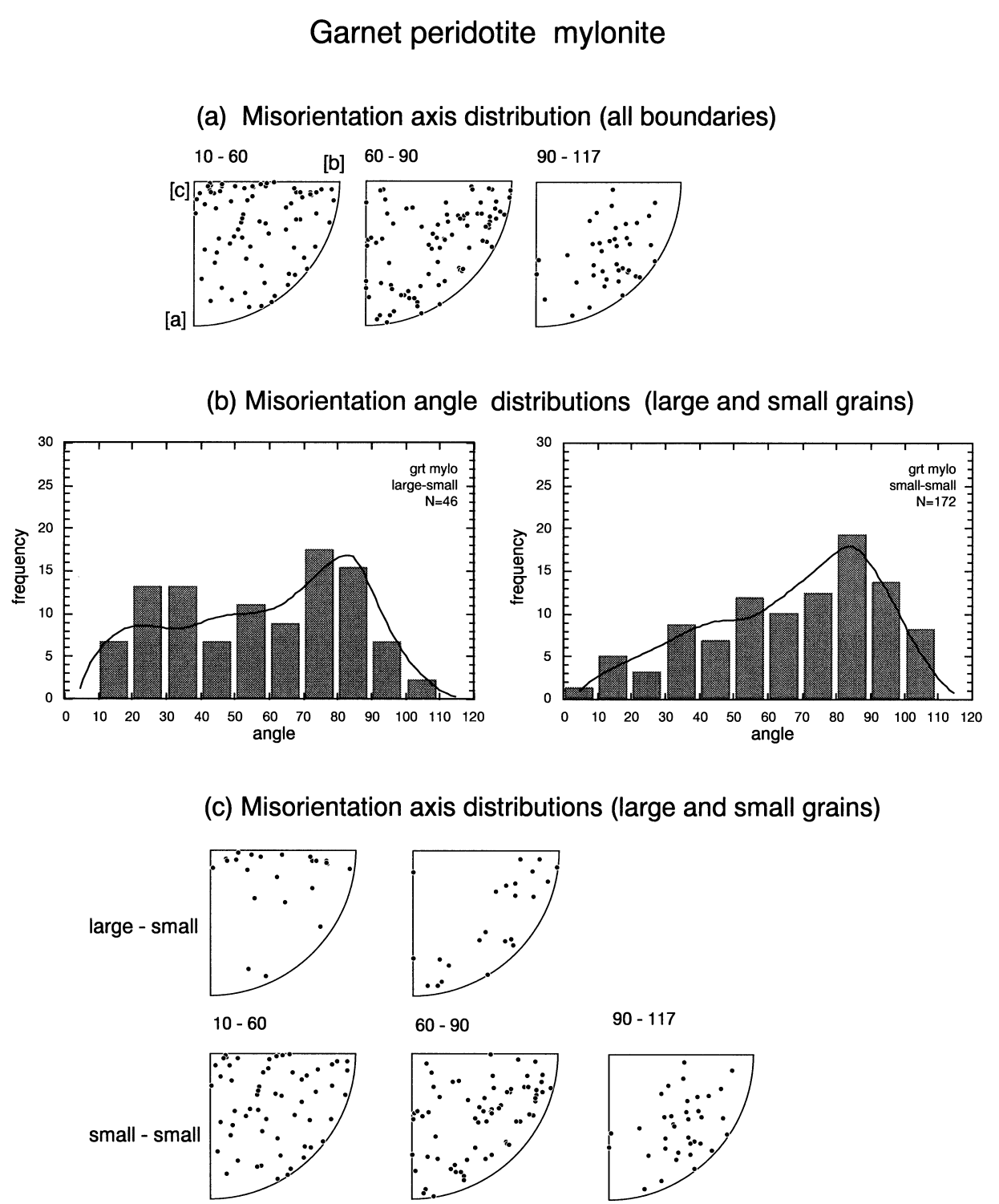
Garnet peridotite mylonite
(a) Misorientation axis distribution (all boundaries)
10 - 60
60 - 90
90 - 117
[b]
[c]
[a]
(b) Misorientation angle distributions (large and small grains)
grt mylo
large-small
N=46
grt mylo
small-small
N=172
frequency
angle
(c) Misorientation axis distributions (large and small grains)
large - small
small - small
10 - 60
60 - 90
90 - 117

6. Discussion

6.1. Influence of deformation mechanism on CPO

Deformation mechanisms are thought to have a strong influence on CPO development. Cold-working and dislocation creep generally results in the development of a strong CPO. In contrast, deformation by dominant grain boundary sliding results in a weak to random CPO in metals (Padmanabhan and Davies, 1980). Data on the CPO formed by diffusion creep and grain boundary sliding in rocks is rather limited. Schmid et al. (1987) and Rutter et al. (1994) report weak, but not random, CPO in calcite polycrystals deformed to large strain by diffusion and grain boundary sliding. Karato (1988) found a weak CPO in an olivine sample deformed to 8% strain in the diffusion creep regime but the significance of that result is limited because of the low strain. Our data confirm that the olivine CPO remains weak to random in the diffusion creep regime at strains up to 24% uni-axial shortening.

Our high-stress dislocation creep sample (5072) has a significant CPO typical for olivine deformed in uni-axial compression (Avé Lallemant and Carter, 1970; Nicolas et al., 1973; Daines and Kohlstedt, 1997). The larger grains have a stronger CPO than the smaller equi-axial grains. The deformation mechanism map in Fig. 2 shows that the small grain size fraction plots close to the transition between diffusion creep and dislocation creep. The weaker CPO in the small grains may be a signature of deformation by a combination of dislocation creep and diffusion creep in the fine-grained fraction.

The lower-stress dislocation creep sample (6223) has been deformed to moderate strain yet the CPO is weak compared to other olivine samples deformed to lower total strains (Karato, 1988; Daines and Kohlstedt, 1997). There is also no difference in the strength of the CPO for large and small grains. Interpretation of this sample is made difficult by its complicated history of deformation and annealing (Table 1). The CPO could be weak for several reasons including (1) low strain, (2) enhanced grain boundary sliding (Zhang et al., 1994) as indicated by the diamond grain structure (Drury and Humpreys, 1988), and (3) weakening of CPO during annealing.

Our results indicate that a significant CPO develops in olivine during deformation involving dislocation creep and dynamic recrystallisation after only 10–20% uni-axial strain (see also Avé Lallemant and Carter, 1970; Karato, 1988; Daines and Kohlstedt, 1997). In contrast, the olivine CPO in the diffusion creep regime remains weak at strains (24%) which are large enough for a significant CPO to form in the dislocation creep regime. These results confirm the commonly used criteria, mainly based on studies from metals, that CPOs in olivine can be used as an indicator of the dominant deformation mechanism. Note that at high strain in the grain boundary sliding and diffusion creep regime a weak CPO may develop (Schmid et al., 1987; Rutter et al., 1994). A possible example of a weak CPO formed by high-strain, grain boundary sliding in a peridotite mylonite is described by Newman et al. (1999).

6.2. Influence of deformation mechanisms on MOD

At present, little is known about the effect of deformation mechanisms on grain MOD. The present study has demonstrated that the strength of an olivine CPO has a major influence on the MOD. For large-strain deformation different deformation mechanisms will produce different CPOs and hence different MODs (Fig. 16). The experimental samples we have studied were deformed to low strain by different deformation mechanisms. In consequence, the CPOs in all samples are relatively weak and the differences in MOD between samples deformed by different deformation mechanisms are not large. Compared with the diffusion creep sample the dislocation creep samples have a higher frequency of intermediate boundaries, a shift in the mode of the MAD to lower angles and a higher frequency of 10–20º misorientation boundaries which may be related to dynamic recrystallisation processes in the dislocation creep samples. At high strains different MODs will develop in samples deformed by different deformation mechanisms (Fig. 16). In the diffusion creep regime the MOD should remain random, while in the dislocation creep regime the MOD will be non-random (Avé Lallemant, 1985) owing to the development of a strong CPO. Some studies of naturally deformed quartz show that the MODs for rocks inferred to deform by diffusion and dislocation creep are very different (Fliervoet et al., 1997, fig. 12).

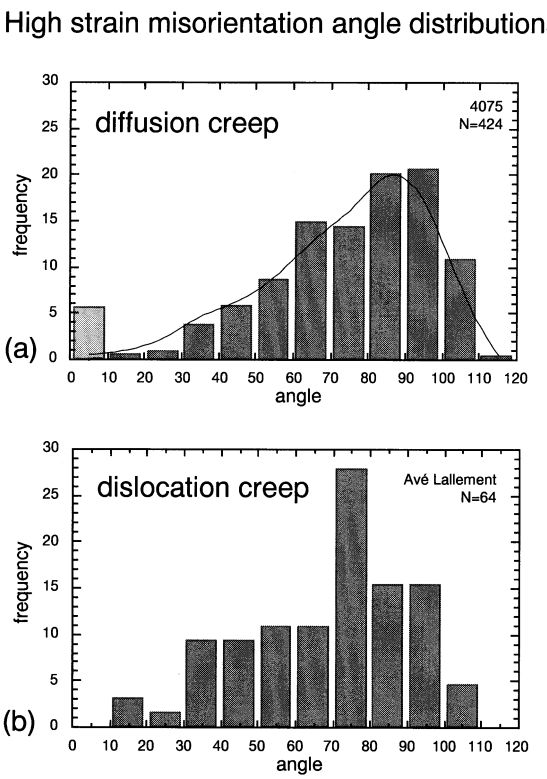

Fig. 16. Some examples of misorientation angle distributions expected for high-strain diffusion creep (a) and dislocation creep with dynamic recrystallisation (b). Misorientations below 10° are designated as subgrains and are shown in a brighter tone. The associated uncorrelated MOD is shown as a thin line; (a) is based on sample 4705 and (b) is from Avé Lallemant (1985).

For quartz rocks deformed by dislocation processes with dominant subgrain rotation recrystallisation the MOD is characterised by low index rotation axes and a tendency for low to intermediate misorientation angles (Lloyd and Freeman, 1994; Fliervoet and White, 1995; Neumann, 1996). These studies suggest that the recrystallisation mechanism also has an important influence on the grain MOD.

6.3. Influence of dynamic recrystallisation on CPO

For recrystallisation by subgrain rotation the CPO of recrystallised grains is expected to be similar to that of the larger old grains (Karato, 1988). A larger effect on CPO is expected if significant grain growth occurs during dynamic recrystallisation (Karato, 1988; Jessel and Lister, 1990). Recrystallisation may influence the CPO in several ways (Humphreys and Hatherly, 1996): (1) preferential growth or nucleation of grains with particular (hard or soft) orientations (Duval, 1979; Toriumi and Karato, 1987; Karato, 1988; Ree, 1990; Wenk et al., 1997); (2) the preferential elimination of particular grain orientations (Burg et al., 1986); and (3) the preferential growth of new grains surrounded by high-mobility, special, grain boundaries, e.g. CSL boundaries in metals (Gordon and Vandermeer, 1966; McLaren, 1986).

The CPOs measured in our study are dominated by small recrystallised grains. The small grain CPOs are broadly similar to the large grain CPOs with similar or slightly rotated maxima (Fig. 7). Similar results have been obtained for rotation recrystallisation in simple shear (Zhang and Karato, 1995) and from naturally deformed rocks (Mercier, 1985; Drury and Van Roermund, 1989). In contrast, Avé Lallemant and Carter (1970) found two types of CPO for recrystallised grains. The CPO of intragranular grains was similar to that of deformed old grains, whereas, the new grains formed at old grain boundaries and totally recrystallised samples had a strong CPO with the [*b*]-axes subparallel to the compression axis. Toriumi and Karato (1987) also found two types of grain in recrystallised olivine single crystals. New grains which had formed by subgrain rotation had a similar orientation to the relict large grain (Karato, 1988). Other dislocation-free grains with a large misorientation from the host, with [*b*] sub-parallel to the compression axis, formed along the new grain boundaries which had previously been produced by subgrain rotation. The growth of hard, dislocation-free, grains with [*b*] sub-parallel to the compression axis could be a case of stress-controlled CPO (Karato, 1988). Note that the stress-controlled CPO model of Karato (1987, 1988) is based on differences in the stored plastic strain energy between grains and is not the same process as *stress-induced* recrystallisation proposed by Kamb (1959). The arguments presented by Nicolas and Poirier (1976, pp. 158–163) against *stress-induced* recrystallisation do not apply to the stress-controlled CPO model (Karato, 1987, 1988).

All of the experimentally deformed samples which show some evidence of preferential growth of recrystallised grains with hard orientations (Avé

Lallemant and Carter, 1970; Kunze and Avé Lallemant, 1981; Toriumi and Karato, 1987; Karato, 1988) were deformed at stresses less than about 100 MPa. In higher-stress samples (Zhang and Karato, 1995; this study) dynamic recrystallisation produces a CPO broadly similar to the old grains. This type of CPO may be explained by the combined effects of crystal plasticity and the preferential growth of recrystallised grains with a soft orientation (e.g. Duval, 1979; Wenk et al., 1997). It is clear that further work is needed to fully understand the effect of recrystallisation and different recrystallisation mechanisms on CPO in olivine rocks.

6.4. Influence of dynamic recrystallisation on MOD

In the olivine rocks investigated in this study, there is evidence for the formation of high-angle subgrains and possibly new grain boundaries by subgrain rotation in the dislocation creep regime. The occurrence of irregular and bulged grain boundaries and the diamond grain structure in sample 6223 indicate that grain boundary migration was also important. The subgrain misorientation axes in samples 5072 and 6223 have general orientations suggesting that the subgrain boundaries form by recovery of [*a*] and [*c*] dislocations. In sample 5072 (high-stress dislocation creep) and the naturally deformed garnet–mylonite, the MOD between large and small grains are non-random. There are more low- to intermediate-angle boundaries than would be expected from the uncorrelated MOD. The misorientation axes of such low- to intermediate-angle boundaries tend to be perpendicular to the [*a*]-axis (garnet mylonite) and the [*b*]-axis for sample 5072. These preferred orientations suggest that the geometrically necessary dislocations which accommodate the misorientations were produced by [*a*]-slip in the garnet mylonite and a combination of [*a*]- and [*c*]-slip in sample 5072. The misorientations for the Dreiser sample (Avé Lallemant, 1985), with a dominance of low- to intermediate-angle boundaries and misorientation axes close to the [*b*]-axes are consistent with dominant subgrain rotation recrystallisation.

The misorientation relationships between large and small grains are characteristic of a host control orientation relationship between new and old grains. Host control can be produced by several types of recrystallisation mechanism. For subgrain rotation the new grains usually retain some orientation relation with the parent grain with many low to intermediate grain misorientations (Hobbs, 1968; White, 1973; Poirier and Nicolas, 1975; White, 1977; Lloyd and Freeman, 1994). The misorientation axis produced by single slip should be parallel to a low index crystal direction (Lambregts and van Roermund, 1990; Buatier et al., 1991; Lloyd and Freeman, 1991, 1994). The misorientation axes of subgrains in regions of multiple slip can have more general directions (Buatier et al., 1991; Lloyd and Freeman, 1994; Lloyd et al., 1997). In most cases subgrain rotation is also associated with significant subgrain boundary or grain boundary migration (Drury et al., 1985; Drury and Urai, 1990; Lloyd and Freeman, 1994). High-angle subgrains can be formed by migration of a subgrain boundary through a region of cumulative lattice curvature (Drury et al., 1985; Urai et al., 1986) or by coalescence of subgrains or grains (Means and Ree, 1988). In these cases the misorientation axis of the new boundary may not be related to the active slip systems, particularly if different slip systems are active in different domains of an old grain. To complicate matters further, once a subgrain boundary has transformed into a grain boundary the occurrence of grain boundary sliding can produce extra rotations which will obscure any preferred misorientations produced by slip (Fliervoet and White, 1995).

New grains nucleated by a combination of migration and rotation processes can also have an orientation relationship with the host old grain (e.g. Avé Lallemant and Carter, 1970; Drury and Van Roermund, 1989, fig. 8). Avé Lallemant (1985) has documented a clear orientation relationship between new grains growing inside old grains with common misorientation angles of 30–60° and 70–90° (his fig. 10). The misorientation axes show no clear preferred orientation. If migration recrystallisation occurs without subgrain or new grain development (Means, 1983; Urai, 1987) new recrystallised grains will grow into their neighbours and no particular orientation relationships would be expected. The related case of preferential growth of new grains surrounded by high-mobility special boundaries (Gordon and Vandermeer, 1966) should be reflected in a high frequency of special misorientations in the MOD.

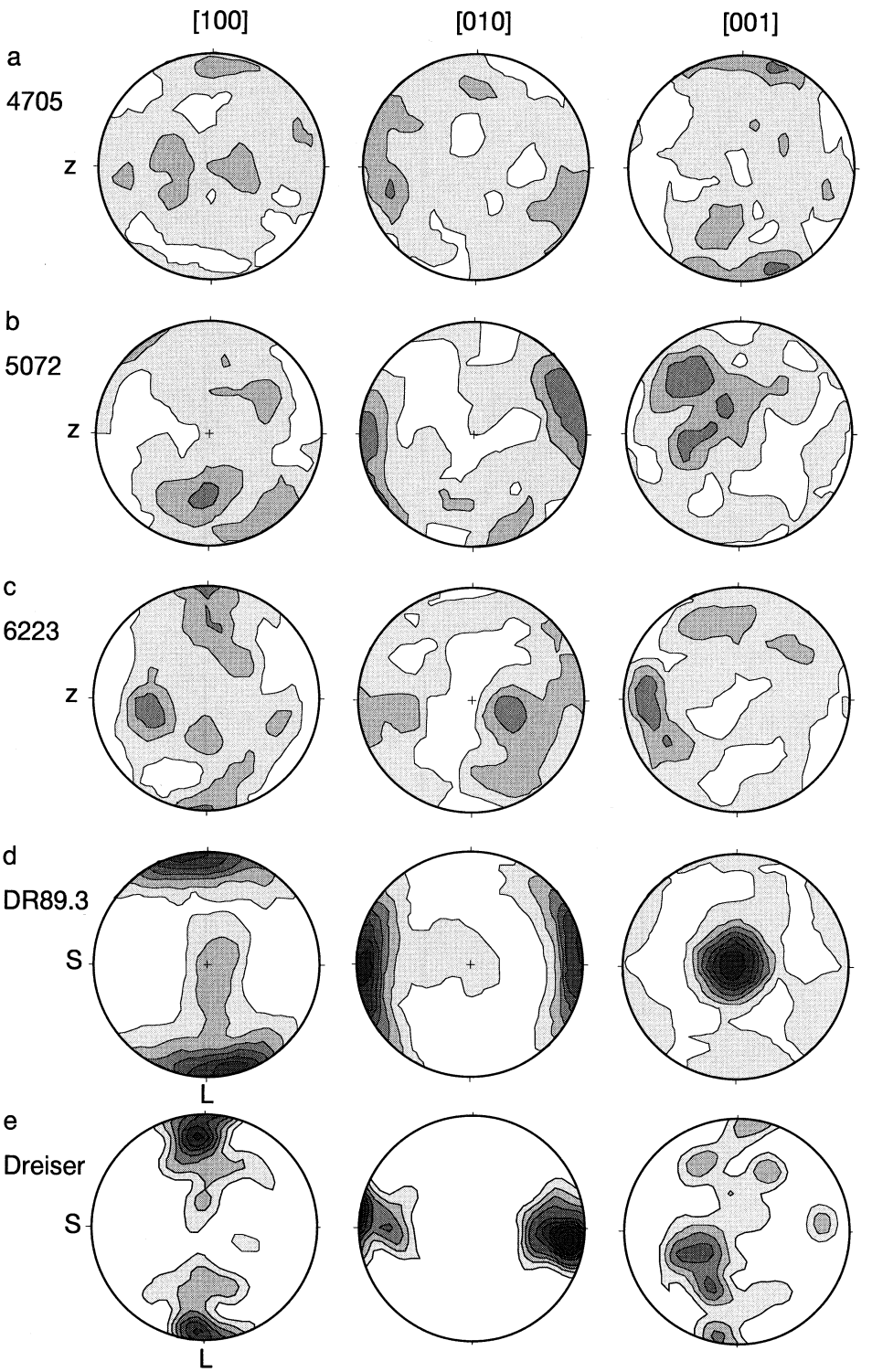
[100]
[010]
[001]
a
4705
z
b
5072
z
c
6223
z
d
DR89.3
S
L
e
Dreiser
S
L

There is no clear evidence for the occurrence of preferred or special misorientation grain boundaries in any of the olivine samples we have investigated in this study. Faul and Fitz Gerald (1999) have found some evidence for the occurrence of some special boundaries characterised by a 60º rotation around the [*a*]-axis. This misorientation corresponds to a CSL boundary for the oxygen sub-lattice.

The microstructures and the host control relationship between old and new grains found in this study suggest that dynamic recrystallisation in the dislocation creep samples occurred by a general recrystallisation mechanism (Drury and Urai, 1990) with nucleation of new grains by a combination of both rotation and migration processes. It is emphasised that, apart from the host control relationship between adjacent large and small grains, the MOD is mainly controlled by the CPO. There is no obvious evidence for the occurrence of preferred misorientation, or special, grain boundaries. The only clear 'signal' of dynamic recrystallisation is present in the misorientation relations between old and new grains. In the completely recrystallised areas the MOD is the same as expected from the CPO and there is no clear signal that can be related to the occurrence of any particular recrystallisation processes.

6.5. The role of deformation mechanism versus recrystallisation mechanisms

Comparison of our results with other studies on CPO and MOD (Buatier et al., 1991; Lloyd and Freeman, 1994; Neumann, 1996; Fliervoet et al., 1997; Lloyd et al., 1997) suggests a preliminary classification for rocks deformed to large strains (Table 2). The CPO produced by migration recrystallisation should be characterised by the occurrence of *orientation families* (Urai et al., 1986), whereas the CPO produced by rotation recrystallisation should be *domainal* (Garcia Celma, 1982; Pauli et al., 1996).

The scheme in Table 2 is speculative and needs to be tested and improved. This scheme mainly applies to the initial stage of dynamic recrystallisation which usually involves some grain size reduction. At high strains once a steady-state microstructure (Means, 1989) has developed, recrystallisation is probably dominated by migration processes such as grain dissection, coalescence and amalgamation (Urai, 1987; Means, 1989). It is clear from Table 2 that there are limitations in the use of statistical representations of MOD data. More information on the deformation and recrystallisation processes may be obtained from a combined analysis of microstructure, CPO and MOD (Lloyd and Freeman, 1994; Heidelbach,

Table 2
Preliminary classification of the relationship between CPO and MOD based on the definitions of recrystallisation mechanisms from Drury and Urai (1990)

Mechanism	CPO	Rotation angle distribution	Rotation axis distribution
Diffusion creep	random to weak	random	random
Migration recrystallisation (no subgrains)	strong with orientation families	controlled by the CPO	controlled by CPO
Migration recrystallisation with high-mobility boundaries (no subgrains)	strong with orientation families	high frequency of special boundaries	high frequency of special boundaries
Migration and rotation with new grain development	strong (domainal?)	more intermediate boundaries than expected from CPO control when old relict grains are present.	weak to some preferred orientation
Dislocation creep and rotation recrystallisation (single slip system)	strong domainal	more low and intermediate boundaries than expected from CPO control	preferred orientations parallel to low index directions
Dislocation creep and rotation recrystallisation (multiple slip systems)	strong domainal	more low and intermediate boundaries than expected from CPO control	weak to some preferred orientation depending on number and activity of slip systems

1994; Kunze et al., 1994; Fliervoet and White, 1995; Neumann, 1996; Trimby and Prior, 1999).

7. Conclusions

(1) In fine-grained olivine rocks experimentally deformed to 17–24% strain at 1200–1300ºC different CPOs and MODs are formed in samples deformed by dislocation creep and diffusion creep. The samples show a trend of increasingly weaker CPO with decreasing flow stress and grain size which may be related to an increasing component of grain boundary sliding.

(2) In the dislocation creep regime a significant CPO is developed after strains of 17%. In contrast, the CPO remains weak to random in the diffusion creep at strains (24%) where a strong CPO would be developed by dislocation creep and dynamic recrystallisation.

(3) In the high-stress dislocation creep sample the small grains formed by dynamic recrystallisation have a weaker CPO than large grains. The weak CPO of small grains is consistent with deformation by a combination of dislocation creep, grain boundary sliding and diffusion creep close to the mechanism transition between dislocation creep and diffusion creep.

(4) The CPO has a strong influence on grain boundary misorientations (MOD). Thus, the deformation mechanism which controls the CPO has an influence on the grain boundary population. In the diffusion creep regime the CPO and MOD are weak to random. In the dislocation creep regime the CPO and MOD are non-random but the MOD is principally controlled by the CPO.

(5) The occurrence of dynamic recrystallisation results in the slight preferential occurrence of intermediate-angle grain boundaries. Further work is needed to determine how the CPO and MOD vary with deformation conditions and recrystallisation mechanisms for large strain deformation.

(6) A preliminary classification of the relationship between CPO, MOD and mechanisms is proposed.

(7) The grain boundaries found in the deformed olivine polycrystals are predominately high-angle boundaries with misorientations between 60 and 117º. No evidence has been found for the occurrence of preferred misorientation, or special, grain boundaries.

Acknowledgements

Part of the experimental deformation studies were supported by an Australian Research Council-QEII fellowship (MRD). Graham Horwood (RSES, ANU) is thanked for technical support. Professor Mervyn Paterson is thanked for providing sample 5072. Harri Kokkonen (RSES, ANU) prepared the excellent thin sections. The electron microscopy studies were conducted at EMSA, the Utrecht University Centre for Electron Microscopy and Structure Analysis. Pim van Maurik (EMSA) is thanked for his contributions to setting up the EBSD–SEM. Dirk van der Wal is thanked for providing data on sample DR89.3. Funding from Philips Electron Optics, Eindhoven (TF), a European Community TMR Marie Curie fellowship (TF) and an NWO-PIONIER subsidy (MRD) are gratefully acknowledged. The two anonymous referees and Holger Stünitz are thanked for constructive criticism of the original paper. This study was conducted as part of the programme of the Dutch national research school, the Vening Meinesz Research School of Geodynamics.

References

Avé Lallemant, H.G., 1985. Subgrain rotation and dynamic recrystallization of olivine, upper mantle diapirism, and extension of the Basin-and-Range Province. Tectonophysics 119, 89–117.

Avé Lallemant, H.G., Carter, N.L., 1970. Syntectonic recrystallization of olivine and modes of flow in the upper mantle. Geol. Soc. Am. Bull. 81, 2203–2220.

Buatier, M., van Roermund, H.L.M., Drury, M.R., Lardeaux, J.M., 1991. Deformation and recrystallization mechanisms in naturally deformed omphacites from the Sesia–Lanzo zone; geophysical consequences. Tectonophysics 195, 11–27.

Burg, J.P., Wilson, C.J.L., Mitchell, J.C., 1986. Dynamic recrystallization and fabric development during the simple shear deformation of ice. J. Struct. Geol. 8, 857–870.

Chopra, P.N., 1986. The plasticity of some fine-grained aggregates of olivine at high pressure and temperature. In: Hobbs, B.E., Heard, H.C. (Eds.), Mineral and Rock Deformation: Laboratory Studies. The Paterson Volume, Am. Geophys. Union, Geophys. Monogr. 36, 25–33.

Daines, M.J., Kohlstedt, D.L., 1997. Influence of deformation

on melt topology in peridotites. J. Geophys. Res. 102 (B5), 10257–10271.
Davis, J.C., 1986. Statistics and Data Analysis in Geology. Wiley, New York.
Drury, M.R., Fitz Gerald, J.D., 1998. Mantle rheology: insights from laboratory studies of deformation and phase transition. In: Jackson, I. (Ed.), The Earth's Mantle:Composition, Structure and Evolution. Cambridge University Press, New York, pp. 503–559.
Drury, M.R., Humpreys, F.J., 1988. Microstructural shear criteria associated with grain-boundary sliding during ductile deformation. J. Struct. Geol. 10, 83–89.
Drury, M.R., Urai, J.L., 1990. Deformation related recrystallization processes. Tectonophysics 172, 235–253.
Drury, M.R., Van Roermund, H.L.M., 1989. Fluid assisted recrystallisation in upper mantle peridotite xenoliths from kimberlites. J. Petrol. 30, 131–152.
Drury, M.R., Humpreys, F.J., White, S.H., 1985. Large strain deformation studies using polycrystalline magnesium as a rock analogue, Part II. Dynamic recrystallisation mechanisms at high temperatures. Phys. Earth Planet. Sci. 40, 208–222.
Duval, P., 1979. Creep and recrystallization of polycrystalline ice. Bull. Minéral. 102, 80–85.
Exner, H.E., 1972. Analysis of grain and particle-size distributions in metallic materials. Int. Metall. Rev. 159, 25–42.
Faul, U., Fitz Gerald, J.D., 1999. Grain misorientations in partially molten olivine aggregates: an electron backscatter diffraction study. Phys. Chem. Miner. (in press).
Fliervoet, T.F., White, S.H., 1995. Quartz deformation in a very fine grained quartzo-feldspathic mylonite: a lack of evidence for dominant grain boundary sliding deformation. J. Struct. Geol. 17, 1095–1109.
Fliervoet, T.F., White, S.H., Drury, M.R., 1997. Evidence for dominant grain boundary sliding deformation in greenschist and amphibolite - grade polymineralic ultramylonites from the Redbank Deformed Zone, central Australia. J. Struct. Geol. 12, 1495–1520.
Forwood, C.T., Clarebrough, L.M., 1991. Electron Microscopy of Interfaces in Metals and Alloys. Electron Microscopy in Materials Science Series, Adam Hilger, Bristol.
Garcia Celma, M.A., 1982. Domainal and fabric heterogeneities in the Cap de Creus quartz mylonites. J. Struct. Geol. 4, 433–455.
Goetze, C., 1978. The mechanisms of creep in olivine. Philos. Trans. R. Soc. London A 288, 99–119.
Gordon, P., Vandermeer, R.A., 1966. Grain boundary migration. In: Margolin, H. (Ed.), Recrystallization, Grain Growth and Textures. ASM, Metals Park, Ohio, pp. 205–266.
Gottstein, G., 1992. Methoden und Anwendungen der lokalen Texturcharakterisierung. Neue Hütte 37, 127–141.
Grimmer, H., 1980. A unique description of the relative orientation of neighbouring grains. Acta Crystallogr. A 36, 382–389.
Heidelbach, F.K., 1994. Textures and Microstructures in Recrystallized Rocks; A Study by X-Ray and Electron Diffraction. PhD. Thesis, University of California.
Hirth, G., Kohlstedt, D.L., 1995. Experimental constraints on the dynamics of the partially molten upper mantle, 2. Deformation in the dislocation creep regime. J. Geophys. Res. 100 (B8), 15441–15449.
Hitchings, R.S., Paterson, M.S., Bitmead, J., 1989. Effects of iron and magnetite additions in olivine-pyroxene rheology. Phys. Earth Planet. Inter. 55, 277–291.
Hobbs, B.E., 1968. Recrystallization of single crystals of quartz. Tectonophysics 6, 353–401.
Humphreys, F.J., Hatherly, M., 1996. Recrystallization and Related Annealing Phenomena. Pergamon Press, London.
Jessel, M.W., Lister, G.S., 1990. A simulation of the temperature dependence of quartz fabrics. In: Knipe, R.J., Rutter, E.H. (Eds.), Deformation Mechanisms, Rheology and Tectonics. Geol. Soc. London Spec. Publ. 54, 353–362.
Kamb, B., 1959. Theory of preferred orientation developed by crystallization under stress. J. Geol. 67, 153–170.
Karato, S.-I., 1987. Seismic anisotropy due to lattice preferred orientations: kinematic or dynamic? In: Manghnani, M.H., Syono, Y. (Eds.), High Pressure Research in Mineral Physics. Am. Geophys. Union, Geophys. Mongr. 39, 455–471.
Karato, S.-I., 1988. The role of recrystallization in the preferred orientation of olivine. Phys. Earth Planet. Inter. 51, 107–122.
Karato, S.-I., Wu, P., 1993. Rheology of the upper mantle: a synthesis. Science 260, 771–778.
Karato, S.I., Paterson, M.S., Fitz Gerald, J.D., 1986. Rheology of synthetic olivine aggregates: influence of grain size and water. J. Geophys. Res. 91 (B8), 8151–8176.
Knipe, R.J., 1989. Deformation mechanisms — recognition from natural tectonites. J. Struct. Geol. 11, 127–146.
Kunze, F.R., Avé Lallemant, H.G., 1981. Non-coaxial experimental deformation of olivine. Tectonophysics 74, T1–T13.
Kunze, K., Adams, B., Heidelbach, F., Wenk, H-R., 1994. Local microstructural investigations in recrystallized quartzite using orientation imaging microscopy. Mater. Sci. Forum 157–164, 965–970.
Lambregts, P.J., van Roermund, H.L.M., 1990. Deformation mechanisms in naturally deformed sillimanites. Tectonophysics 179, 371–378.
Lloyd, G.E., Ferguson, C.C., 1986. A spherical electron-channeling pattern map for use in quartz petrofabric analysis. J. Struct. Geol. 8, 517–526.
Lloyd, G.E., Freeman, B., 1991. Dynamic recrystallization of a quartz porphyroclast. Textures Microstructures 14–18, 751–756.
Lloyd, G.E., Freeman, B., 1994. Dynamic recrystallization under greenschist facies conditions. J. Struct. Geol. 16, 867–881.
Lloyd, G., Law, R.D., Schmid, S., 1987. A spherical channeling pattern map for use in quartz petrofabric analysis: correction and verification. J. Struct. Geol. 9, 251–253.
Lloyd, G.E., Farmer, A.B., Mainprice, D., 1997. Misorientation analysis and the formation and orientation of subgrain and grain boundaries. Tectonophysics 279, 55–77.
Mainprice, D., Lloyd, G.E., Casey, M., 1993. Individual orientation measurements in quartz polycrystals: advantages and limitations for texture and petrophysical property determinations. J. Struct. Geol. 15, 1169–1187.
McLaren, A.C., 1986. Some speculations on the nature of high

angle grain boundaries in quartz rocks. In: Hobbs, B.E., Heard, H.C. (Eds.), Mineral and Rock Deformation: Laboratory Studies. The Paterson Volume. Am. Geophys. Union, Geophys. Monogr. 36, 233–245.

Means, W.D., 1983. Microstucture and micromotion in recrystallization flow of octachloropropane: a first look. Geol. Rundsch. 72, 511–528.

Means, W.D., 1989. Synkinematic microscopy of transparent polycrystals. J. Struct. Geol. 11, 163–174.

Means, W.D., Ree, J.H., 1988. Seven types of subgrain boundaries in octachloropropane. J. Struct. Geol. 10, 765–770.

Mercier, J.-C., 1985. Olivine and pyroxene. In: Wenk, H.-R. (Ed.), Preferred Orientation in Deformed Metals and Rocks: An Introduction to Modern Texture Analysis. Academic Press, Orlando, Calif., pp. 407–430.

Neumann, B., 1996.Texturbildende Prozesse in rekristallisierten Quarzpolykristallen — Einzelkorn- und Gesamttexturanalysen. Geotektonische Forschungen 87, Schweitzerbart, Stuttgart, 154 pp.

Newman, J., Lamb, W.M., Drury, M.R., Vissers, R.L.M., 1999. Deformation processes in a peridotite shear zone: reaction-softening by an H_2O-deficient, continuous net transfer reaction. Tectonophysics 303, 193–222 (this volume).

Nicolas, A., Poirier, J.P., 1976. Crystalline Plasticity and Solid State Flow in Metamorphic Rocks. Wiley-Interscience, London.

Nicolas, A., Boudier, F., Bouiller, A.-M., 1973. Mechanisms of flow in naturally and experimentally deformed peridotites. Am. J. Sci. 273, 853–876.

Padmanabhan, K.A., Davies, G.J., 1980. Superplasticity. Materials Research and Engineering. Springer-Verlag, Berlin.

Palumbo, G., Aust, K.T., 1992. Special properties of Σ grain boundaries. In: Wolf, D., Yip, S. (Eds.), Materials Interfaces: Atomic-Level Structure and Properties, XIV–XVIII. Chapman and Hall, London.

Pauli, C., Schmid, S.M., Panozzo Heilbronner, R., 1996. Fabric domains in quartz mylonites: localized three dimensional analysis of microstructure and texture. J. Struct. Geol. 18, 1183–1203.

Poirier, J.P., Nicolas, A., 1975. Deformation induced recrystallization due to progressive misorientation of subgrains with special reference to mantle peridotites. J. Geol. 83, 707–720.

Poirier, J.P., Vergobbi, B., 1978. Splitting of dislocations in olivine, cross-slip-controlled creep and mantle rheology. Phys. Earth Planet. Inter. 16, 370–378.

Prior, D.J., Trimby, P.W., Weber, U.D., Dingley, D.J., 1996. Orientation contrast imaging of microstructures in rocks using forescatter detectors in the scanning electron microscope. Mineral. Mag. 60, 859–869.

Randle, V., 1992. Microtexture Determination and its Applications. Institute of Materials, London.

Randle, V., 1993. The Measurement of Grain Boundary Geometry. Electron Microscopy in Materials Science Series, IOP, Bristol.

Randle, V., Ralph, B., 1986. A practical approach to the determination of the crystallography of grain boundaries. J. Mater. Sci. 21, 3823–3828.

Ree, J.H., 1990. High temperature deformation of octachloropropane:dynamic grain growth and lattice reorientation. In: Knipe, R.J. Rutter, E.H. (Eds.), Deformation Mechanisms Rheology and Tectonics. Geol. Soc. London Spec. Publ. 54, 363–368.

Reimer, L., 1985. Scanning Electron Microscopy. Springer Series in Optical Sciences, Springer-Verlag, Berlin.

Rutter, E.H., Casey, M., Burlini, L., 1994. Preferred crystallographic orientation development during the plastic and superplastic flow of calcite rocks. J. Struct. Geol. 16, 1431–1446.

Schmid, S.M., Panozzo, R., Bauer, S., 1987. Simple shear experiments on calcite rock: rheology and microfabric. J. Struct. Geol. 9, 774–778.

Schmidt, N.-H., Olesen, N.O., 1989. Computer-aided determination of crystal-lattice orientation from electron-channeling patterns in the SEM. Can. Mineral. 27, 15–22.

Schwarzer, R.A., Weiland, H., 1988. Texture analysis by the measurement of individual grain orientations — electron microscopical methods and application on dual phase steel. Textures Microstructures 8–9, 551–577.

Schwarzer, R.A., 1990. Measurement of local textures with transmission electron and scanning electron microscopes. Textures Microstructures 13, 15–30.

Toriumi, M., Karato, S.-I., 1987. Preferred orientation development of dynamically recrystallized olivine during high temperature creep. J. Geol. 93, 407–417.

Trimby, P., Prior, D., 1999. Microstructural imaging techniques — a comparison between light and scanning electron microscopy. Tectonophysics 303, 71–81 (this volume).

Turner, F.J., Weiss, V., 1963. Structural Analysis of Metamorphic Tectonites. McGraw-Hill, New York.

Underwood, E.E., 1970. Quantitative Stereology. Addison-Wesley, Reading, Mass.

Urai, J.L., 1987. Development of microstructure during deformation of carnallite and bischofite in transmitted light. Tectonophysics 135, 251–263.

Urai, J.L., Means, W.D., Lister, G.S., 1986. Dynamic recrystallization of minerals. In: Hobbs, B.E., Heard H.C. (Eds.), Mineral and Rock Deformation: Laboratory Studies. The Paterson Volume. Am. Geophys. Union, Geophys. Monogr. 36, 161–199.

Van der Wal, D., 1993. Deformation Processes in Mantle Peridotites. PhD. Thesis, Geol. Ultraiectina 102, Utrecht University.

Van der Wal, D., Dingley, D.J., 1996. An introduction to EBSP. Philips Electron Optics Bull. 134, 19–25.

Venables, J.A., Harland, C.J., 1973. Electron back-scattering pattern — a new technique for obtaining crystallographic information in the scanning electron microscope. Philos. Mag. 27, 1193–1200.

Wenk, H.R. (Ed.), 1985. Preferred Orientations in Deformed Metals and Rocks: An Introduction to Modern Texture Analysis. Academic Press, Orlando, Calif.

Wenk, H.-R., Canova, G., Bréchet, Y., Flandin, L., 1997. A deformation based model for recrystallization of anisotropic materials. Acta Mater. 45, 3283–3296.

White, S.H., 1973. Syntectonic recrystallization and texture development in quartz. Nature 244, 267–268.

White, S.H., 1976. The effects of strain on the microstructures, fabrics, and deformation mechanisms in quartzites. Philos. Trans. R. Soc. London A 283, 69–86.

White, S.H., 1977. Geological significance of recovery and recrystallization processes in quartz. Tectonophysics 39, 143–170.

Wolf, D., Merkle, K.L., 1992. Correlation between the structure and energy of grain boundaries in metals. In: Wolf, D., Yip, S. (Eds.), Materials Interfaces: Atomic-Level Structure and Properties. Chapman and Hall, London, pp. 87–150.

Woodcock, N.H., 1977. Specification of fabric shapes using an eigenvalue method. Geol. Soc. Am. Bull. 88, 1231–1236.

Zhang, S., Karato, S.-I., 1995. Lattice preferred orientation of olivine aggregates deformed in simple shear. Nature 375, 774–777.

Zhang, Y., Hobbs, B.E., Jessell, M.W., 1994. The effect of grain boundary sliding on fabric development in polycrystalline aggregates. J. Struct. Geol. 16, 1315–1325.